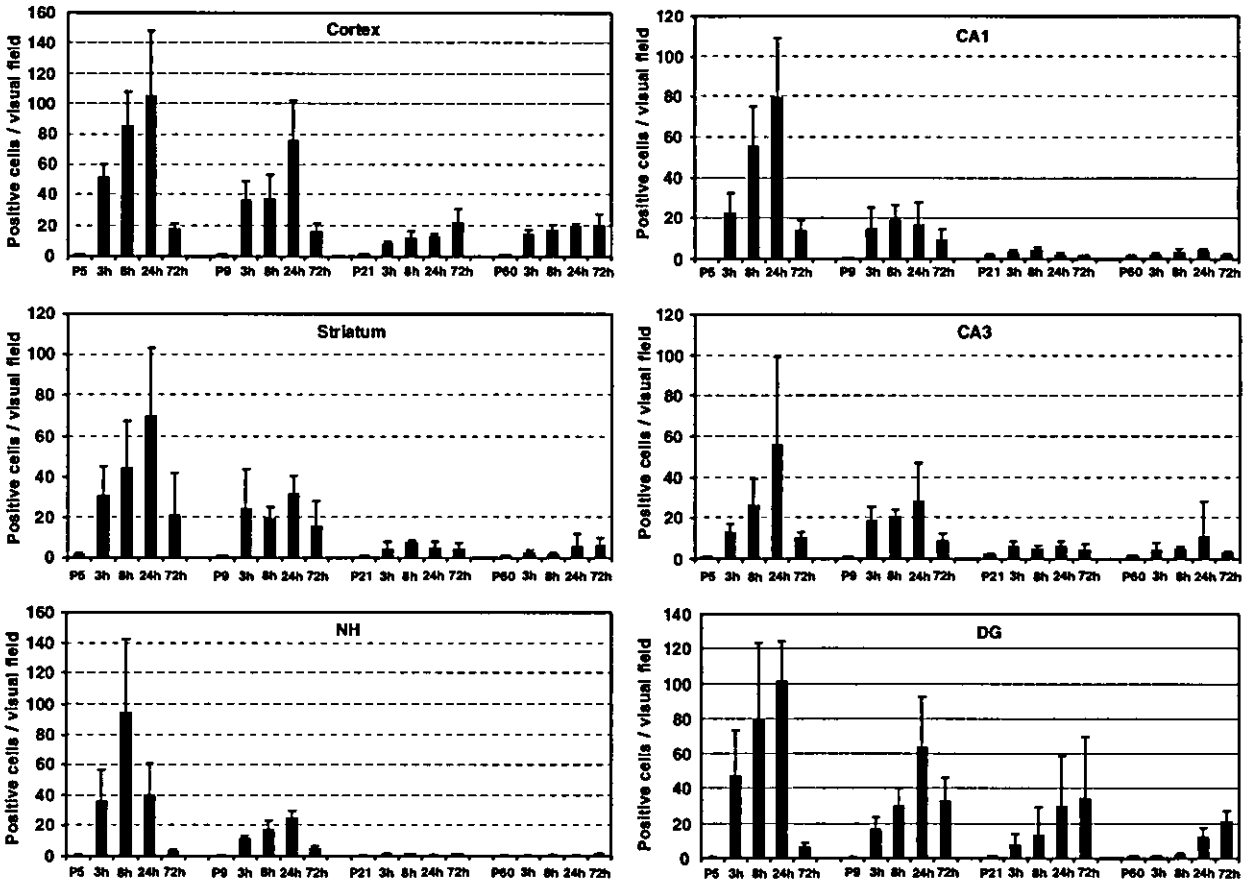

Figure 3 Counts of AIF-positive cells in the ipsilateral hemisphere after HI. AIF-positive cells (as shown in Figure 2c) displayed conspicuous cytosolic and/or nuclear immunostaining. Cells were counted in the cortex, striatum, the NH of the thalamus and the CA1, CA3 as well as DG of the hippocampus. Data are presented as mean ± s.d ($n = 6$ animals per time point). The patterns of AIF immunostaining appeared to follow the time course for development of injury in the selected brain regions for P5 and P9, but not for P21 and P60. The number of AIF-positive cells in the cerebral cortex peaked at 24 h post-HI for both P5 and P9 mice, but there was no dramatic increase in AIF-positive cells in the injured areas of P21 and P60 mice. The lack of AIF-positive cells in the NH of P21 and P60 mice reflects the lack of injury in this region at these ages

HI (Figure 8f). FBDP-positive cells accumulated and reached a peak in injured and borderline regions ipsilaterally as early as 3 h post-HI in the cortex, striatum and NH of P5 mice (Figure 9). FBDP-positive cells appeared in a somewhat delayed fashion in P60 mice in those regions (Figure 9). In the hippocampus, especially in the CA1, unlike the cortex, very few FBDP-positive cells could be detected in P5 and P9 animals, but more positive cells were observed in P21 and P60 animals (Figure 9).

Nitrotyrosine formation after HI

Both nNOS and iNOS showed a similar developmental pattern, displaying approximately three-fold higher protein levels at P5 than P60 (Figure 10a and b). In tissue sections, NOS-dependent, peroxynitrite-mediated nitrotyrosine immunoreactivity was mainly located in the nuclei of injured cells (Figure 10c). The number of nitrotyrosine-positive cells increased immediately after HI and reached a peak around 8–24 h in most of the brain regions (Figure 11), as described earlier.[38] The number of nitrotyrosine-positive cells did not vary appreciably between the different ages (Figure 11). The lack of staining in the NH reflected its resistance to HI, as in the case of all the other staining. The only injured area that displayed a developmental difference was the DG, having fewer positive cells in the juvenile and adult brains (Figure 11).

Autophagy after HI

Immunoblots of homogenates using an antibody against microtubule-associated protein 1 light chain 3 (LC3) showed that LC3-I (16 kDa) was abundant in the brain. LC3-I is cytosolic, whereas LC3-II (14 kDa) is membrane-bound, and the amount of LC3-II is correlated with the extent of autophagosome formation.[26] Both LC3-I and LC3-II could be detected in normal control brains, more pronounced in the immature brains, and both forms were significantly lower in normal adult brains (Figure 12a). After HI, LC3-II increased in the ipsilateral hemisphere, and this process appeared to peak 24–72 h after HI (data not shown). The relative increase of LC3-II in the ipsilateral hemisphere was more pronounced in the adult than the immature brain, approximately three-fold

NPG.CDD.4401545

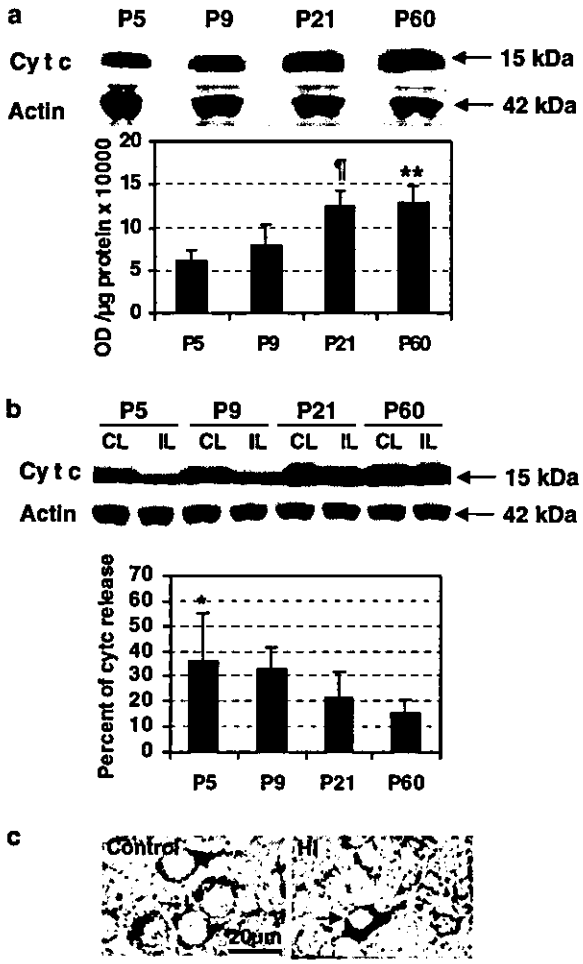

Figure 4 Cyt *c* release from mitochondria after HI. (**a**) The top panel shows representative immunoblots of homogenate samples stained with an antibody against Cyt *c*. The middle panel shows equal loading by actin staining. The lower panel shows the results from densitometric quatifications, demonstrating that Cyt *c* increased significantly during development (**$P<0.01$ and ¶$P<0.01$ compared with P5 and P9). (**b**) Cyt *c* was released from the mitochondrial fraction after HI in the ipsilateral (IL) compared with the contralateral (CL) hemisphere at 24 h post-HI, more pronounced in the immature brains (*$P<0.05$ compared with P60). The actin staining on the same membrane verified equal loading. (**c**) Typical immunostaining of Cyt *c* in control and postischemic (HI) tissue. An injured, Cyt *c*-positive cell is indicated by an arrow in the right panel. Bar = 20 μm

higher compared with normal controls, somewhat less compared with the contralateral hemispheres (Figure 12b).

Discussion

The influence of age on HI brain injury

The developing brain has been reported to be more resistant to certain insults than its adult counterparts.[1,3] The reason for increased susceptibility to injurious stimuli in older brains is often attributed to increased metabolic requirements once connectivity is complete.[39] Other experimental studies question these conclusions.[4,8,9,40] McDonald *et al*.[8] injected NMDA into the striatum of 7-day- and 3-month-old rats, producing 21 times larger damage in the younger animals than in the adults,[8] which reflects the higher density of NMDA receptors in the developing brain. Similarly, Ikonomidou *et al*.[9] demonstrated that the vulnerability to HI peaked at P6, and diminished thereafter. Yager *et al*., using male rats exposed to identical HI insults, demonstrated that brain damage was most severe in 1- and 3-week-old animals, followed by those that were 6 months old. The 6- and 9-week-old animals had significantly less injury than the other age groups.[4] Our results are consistent with the apprehension that immature brains are considerably less susceptible to HI injury than mature ones. The two independent methods used to evaluate brain injury in this study have been shown to correlate well with each other.[41–43] Our results showed that longer hypoxia times were required to obtain a similar degree of brain injury in the immature brains than in the older ones. Furthermore, in the immature brain, extensive atrophy was observed, that is, in addition to the acute loss of dead tissue, there was secondary loss of tissue because the acutely lost tissue could not support the further growth of the surrounding brain tissue. Using the different durations of hypoxia, both the extent and distribution of brain injury was very similar, with a couple of exceptions. The NH was virtually resistant to HI injury in P60 mice, whereas in the immature brain, this area is one of the first to display signs of tissue damage, such as loss of MAP-2. The CA1 has earlier been reported to be relatively resistant to HI in the immature brain, and the selective vulnerability of this subfield developed between P13 and P21 in rats.[3] In the present study, the CA1 was injured at all ages; however, the mechanisms involved appeared to change dramatically between P5 and P21, shifting from mainly AIF translocation, Cyt *c* release and caspase-3 activation at P5, to mainly calpain activation at P21 and P60. It is clear that the vulnerability of the brain is strongly influenced by age, although the mechanisms behind these developmental changes are only partly understood.[2,9,22,44]

The influence of age on cell death mechanisms

Activation of caspase-3 appears to be a critical event in the execution of neuronal apoptosis in the brain during development and after acute injury.[1,21,23–25] In this study, we examined caspase-3 during normal development and after HI. We demonstrated that caspase-3 decreased dramatically during normal development of the mouse brain as judged by the basal activity and by immunoblotting, consistent with our previous reports from the rat brain.[16,23,32] This developmental downregulation of caspase-3, as well as downregulation of other elements involved in caspase-3 activation, such as Apaf-1 and bax, occurs in parallel with the decline of physiological programmed cell death and may serve as a supplementary mechanism protecting the mature brain from apoptosis.[17,18,40] Accordingly, caspase-3 activity increased dramatically after HI in the immature brain but increased only slightly in the mature brain. Immunostaining of active caspase-3 showed very few positive cells in most regions of the adult brain, indicating that caspase-3-mediated neuronal death does not play a major role in the mature brain after HI, in accordance with earlier findings.[1,27] In support of our findings,

NPG.CDD.4401545

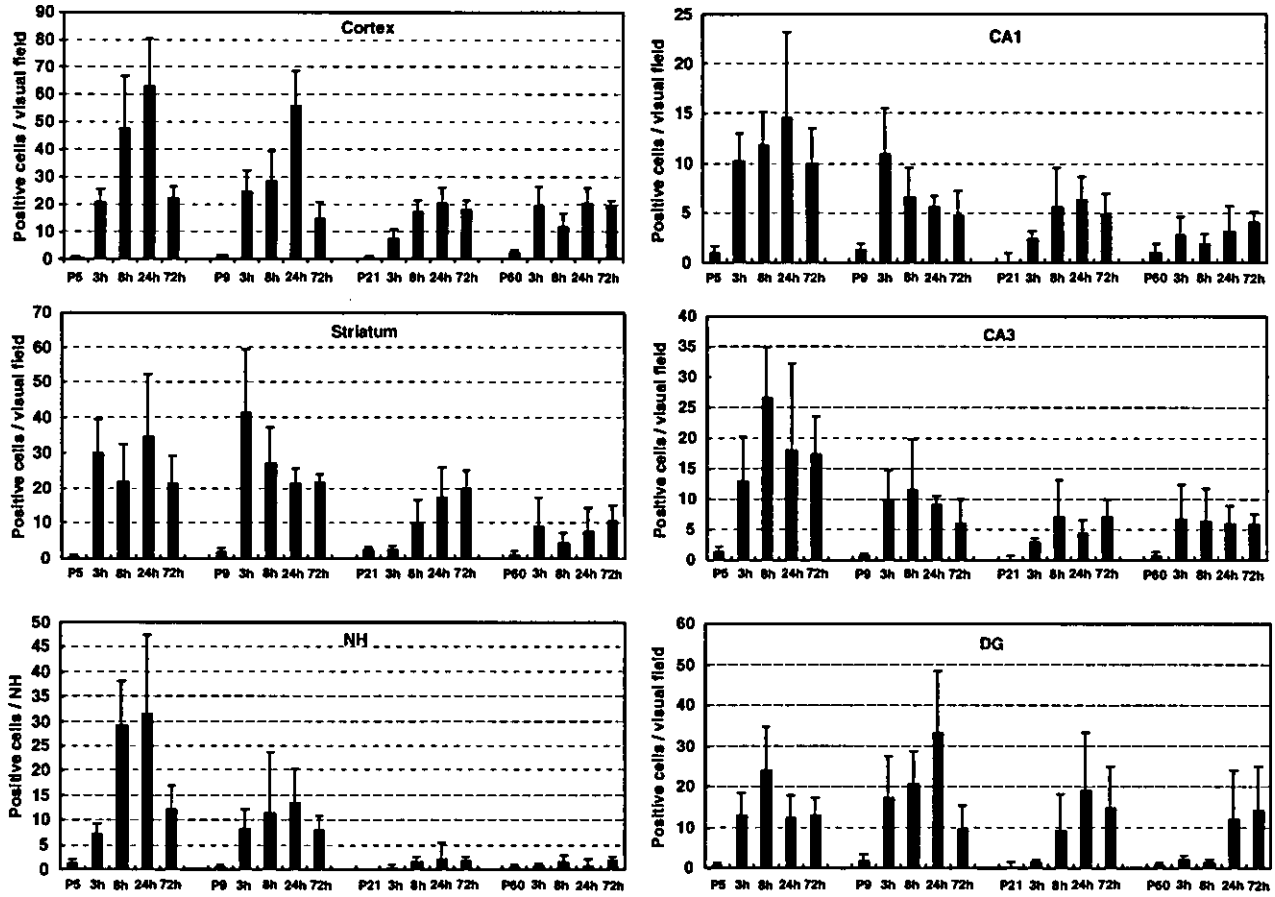

Figure 5 Counts of Cyt *c*-positive cells in the ipsilateral hemisphere after HI. Cyt *c*-positive cells were counted in six different regions as in Figure 3. The total number of positive cells was higher after HI in the younger animals (P5, P9) in most of the regions, displaying a pattern similar to that of the AIF counts in Figure 3

Pohl *et al*.[45] found a marked decrease with age in the extent of distant, apoptosis-related cell death after traumatic brain injury.

Cyt *c* is an essential component of the respiratory chain, an ATP-generating system in the inner mitochondrial membrane. We found that the relative content of Cyt *c* increased during brain development, in agreement with earlier findings.[32,46] This fits with the increased energy requirement in the mature brain needed to maintain the elaborate network of axons and dendrites. Release of Cyt *c* from mitochondria as a consequence of HI has been detected by immunoblotting and immunohistochemistry.[32,47] In some of the affected cells, the staining was associated with DNA fragmentation suggesting apoptosis.[32,48] Other studies showed that loss of mitochondrial Cyt *c* was correlated with an increased production of reactive oxygen species by mitochondria, which may contribute to cellular damage.[49,50] In this study, there were fewer cells displaying increased cytoplasmic Cyt *c* staining in most regions of the mature brains than in the immature brains, indicating that Cyt *c*-related, caspase-3-dependent apoptotic cell death in the mature brain is not as prevalent as in the immature brain.

Caspases have been recognized as important mediators of apoptotic cell death after HI brain injury.[24] However, caspase inhibition has typically resulted in limited neuronal protection.[32,51] This indicates that additional or caspase-independent pathways of neuronal cell death exist. AIF was identified as a major player in caspase-independent cell death.[52] Genetic targeting of AIF abolished the first wave of apoptosis that is indispensable for early embryonic morphogenesis.[53] The expression of AIF in the normal rat brain was reported to decrease slightly with development. However, the protein expression in the cerebellum was markedly increased, distinctively different from the mRNA expression.[54] In the normal rat brain, not including the cerebellum, we found no changes of total AIF protein during the normal brain development.[32] In this study, similar results were found using the mouse brain. So, the constant levels of AIF and increasing levels of mitochondrial markers demonstrated a relative downregulation of AIF with age.[32] Mitochondrial release and nuclear translocation of AIF correlating with neuronal apoptotic cell death have been demonstrated in different brain injury models.[32,33,54–58] In this study, the total number of AIF-positive nuclei decreased in all brain regions and at all the time points with increasing age after HI, indicating that AIF plays a more important role in the early development of neuronal apoptosis. Blocking AIF function with neutralizing antibodies provided significant protection against neuronal cell death.[59]

Downregulation of AIF by RNA interference could inhibit UVA-induced cell death[60] and oxygen/glucose deprivation-induced death of primary cultured neurons (authors' unpublished observations). AIF also has a potent oxidoreductase function[61] and the Harlequin mouse, expressing 80% lower levels of AIF, displayed increased amounts of hydroperoxides in the brain, cerebellum and heart.[62] In summary, accumulating evidence suggests that AIF plays an important role both in normal development and under pathological conditions.

Calpains represent a class of cytosolic cysteine proteases activated by elevated intracellular calcium concentrations. Under pathological conditions, calpains have been implicated in excitotoxic neuronal injury and HI brain injury.[16,31,35–37,63,64] Calpains are activated early in situations of energy depletion and increased calcium influx, triggering other downstream events leading to neurodegeneration. Calpains are generally considered to be activated during excitotoxic and other necrosis-related conditions.[65] Fodrin is a well-known calpain substrate and detection of specific FBDP has been widely used to detect calpain activity.[16,36,37,63,66,67] In this study, FBDP-positive cells increased and reached a peak 3 h post-HI in the cortex, striatum and nucleus habenularis in the immature brain, probably indicating early, necrosis-related cell death. However, in the mature brain, the activation of calpains occurred later, as judged by the later-appearing FBDP, and remained on a high level even at 72 h postinsult, a time point by which there were almost no FBDP-positive cells left in any region of the immature brain. This may indicate sustained calpain activation resulting in lysosomal rupture, causing neuronal necrosis.[68]

Nitric oxide (NO) is produced by three isoforms of nitric oxide synthase (NOS). Inducible and neuronal NOS (iNOS and nNOS, respectively) activities have been demonstrated to increase in models of HI in the immature brain.[69–71] Excessive NO produced after HI combines rapidly with superoxide to form the powerful oxidizing agent peroxynitrite ($ONOO^-$). The $ONOO^-$ adduct is freely diffusible in its protonated form, oxidizes thiol groups, damages mitochondrial respiration and induces protein nitrosylation. Nitrosylation of tyrosine residues in proteins yields the compound 3-nitrotyrosine, and immunohistochemical detection of nitrotyrosine can be used as an indicator of peroxynitrite formation after HI.[38] Pharmacological inhibition nNOS and iNOS reduced nitrotyrosine formation[38] and was demonstrated to be neuroprotective.[72] Oxidative stress, including production of NO and peroxynitrite, is considered to induce mainly necrotic cell death but may also be involved in apoptosis.[73] The developing brain may be

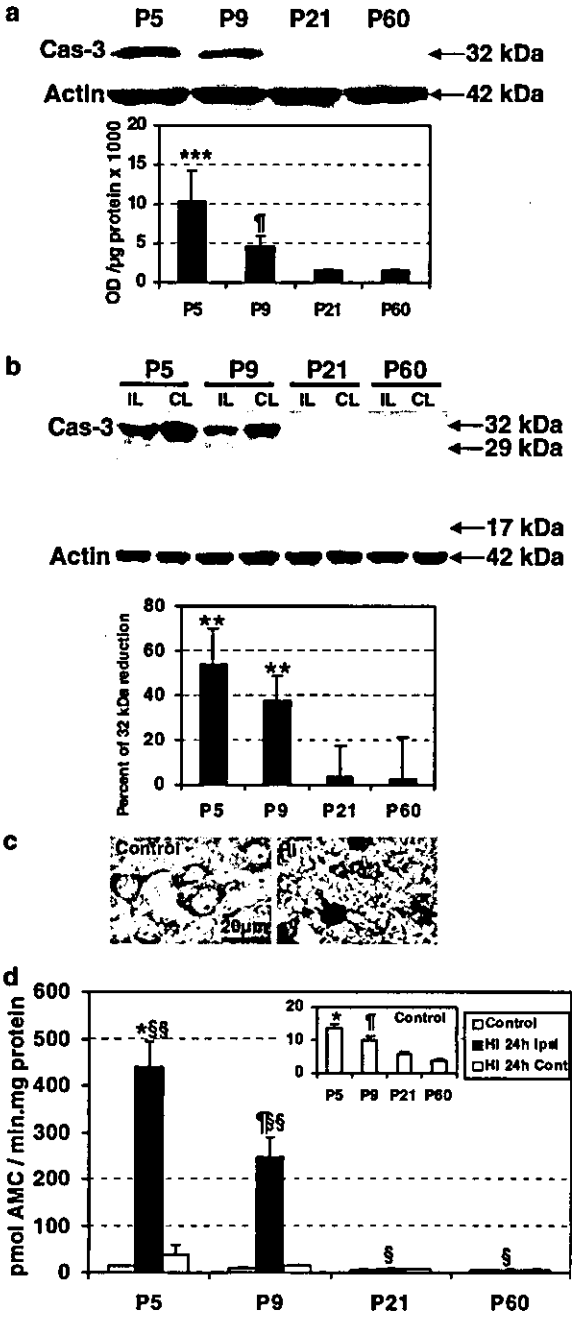

Figure 6 Caspase-3 activation after HI. (a) The 32 kDa proform of caspase-3 decreased during development. There was no significant difference between P21 and P60. (***$P<0.001$ compared with P9, P21 and P60; ¶$P<0.001$ compared with P21 and P60.) The actin staining on the same membrane verified equal loading. (b) After HI, the proform was cleaved and produced 29 and 17 kDa fragments in the ipsilateral (IL), but not in the uninjured contralateral (CL), hemisphere in the P5 and P9 mice. Densitometric quantification showing the relative loss of the 32 kDa proform demonstrated a greater decrease in the P5 and P9 brains (**$P<0.01$ compared with P21 and P60). The actin staining on the same membrane verified equal loading. (c) Typical immunostaining of active caspase-3 c in control and postischemic (HI) tissue. An injured, active caspase-3-positive cell is indicated by an arrow in the right panel. Bar = 20 μm. (d) Crude cytosolic fractions from naïve P5, P9, P21 and P60 ($n=5$ for each age) control animals (Control), and from animals subjected to HI, were assayed for their ability to cleave a fluorogenic peptide substrate (DEVD), reflecting the caspase-3-like activity. All animals subjected to HI were killed 24 h post-HI. The data represent the average from five male animals in each group ± S.D. The activity decreased significantly during development in the normal, control brains (small panel) (*$P<0.0001$ compared with P9, P21, P60; ¶$P<0.001$ compared with P21, P60). After HI, the activity increased significantly at 24 h post-HI in all the groups in the ipsilateral (Ipsi) compared with normal controls, much more pronounced for P5 (31-fold increase) and P9 mice (25-fold increase). The increase was not nearly as pronounced in P21 and P60 mice (§§$P<0.0001$ and §$P<0.05$ compared with the normal controls in the same age group; *$P<0.0001$, compared with P9, P21, P60; ¶$P<0.001$, compared with P21, P60)

NPG.CDD.4401545

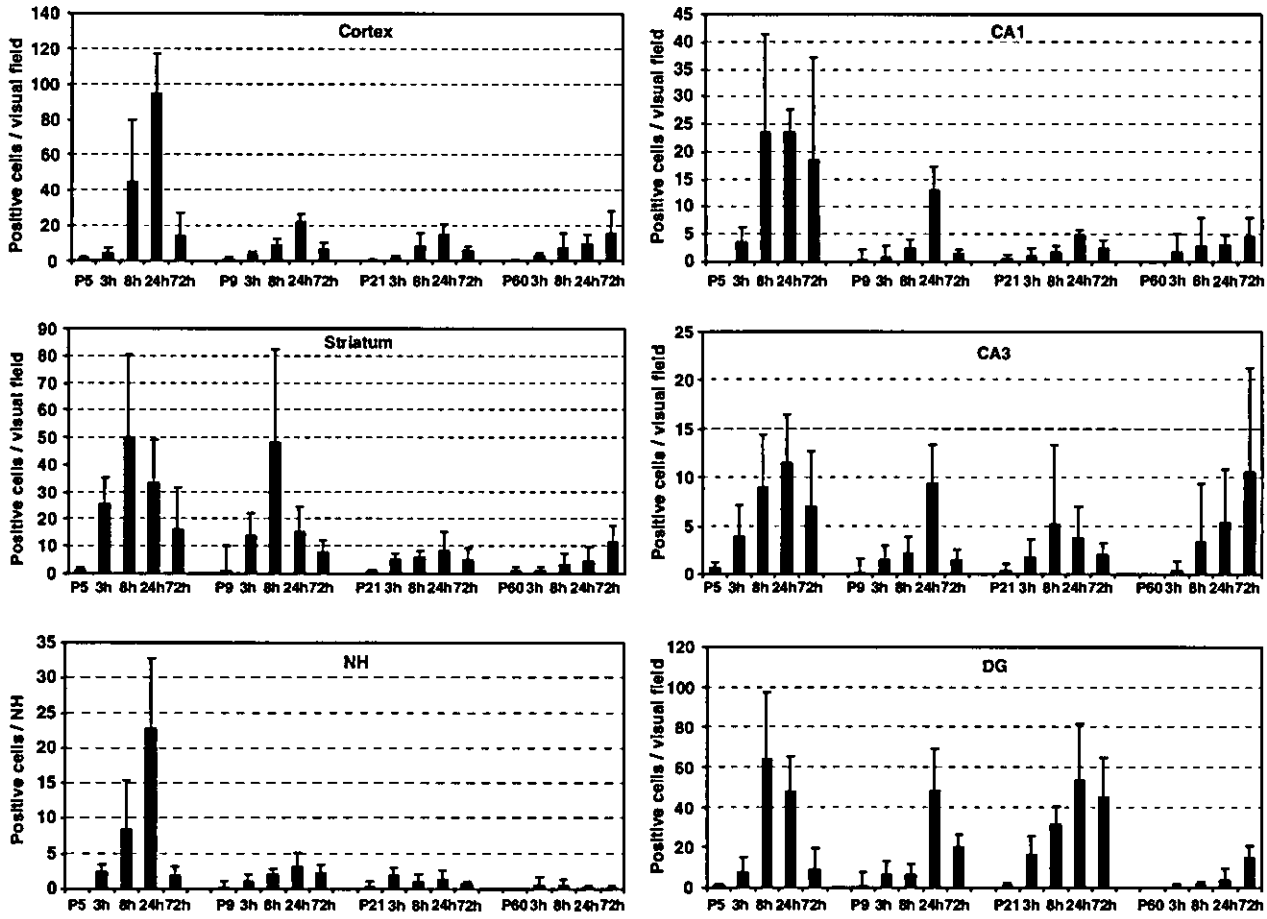

Figure 7 Counts of active caspase-3-positive cells in the ipsilateral hemisphere after HI. Active caspase-3-positive cells were counted in six different regions as in Figures 3 and 5. In most regions, the number of caspase-3-positive cells increased from 3 h and reached a peak at 24 h in the cortex of P5, P9 and P21 animals, but at 72 h for P60 mice

particularly vulnerable to oxidative damage because of its high concentrations of unsaturated fatty acids, high rate of oxygen consumption, low concentrations of antioxidants, and increased availability of 'free' redox-active iron.[74] In this study, however, the extent of nitrotyrosine formation after HI was similar at all ages, despite downregulation of both nNOS and iNOS protein during development. Notably, the levels of iNOS were constitutively high in the immature brain even in naïve control animals.

Autophagy is a process responsible for the bulk degradation of intracellular material in double or multiple-membrane autophagic vesicles, and their delivery to and subsequent degradation by the cell's own lysosomal system. Just like the genetically controlled, physiological programmed cell death, autophagy was demonstrated to be more pronounced during embryonic development and tissue remodeling.[75] One study suggests that autophagy is a caspase-independent, genetically controlled cell death.[76] Visualization of autophagic vesicles by electron microscopy is still the golden standard to demonstrate that autophagy is taking place. The electrophoretic mobility change of LC3 from the nonautophagic, cytosolic form (LC3-I; 16 kDa) to the autophagic, membrane-recruited form (LC3-II; 14 kDa) provides the first molecular marker-based method for detection of autophagic activity.[26,77–79] The notion that autophagy is involved in tissue remodeling is in agreement with our finding that the basal levels of LC3-II in normal control animals was 2.5 times higher in the immature than in the adult brains. After HI, increased LC3-II levels were detected as early as 8 h, much more pronounced after 24 and 72 h. This indicates that autophagy is involved in delayed cell death. Notably, a recent EM study demonstrated numerous vacuoles in degenerating neurons.[80] Even though the basal levels of LC3-II were higher in the immature brains, the increase after HI was more pronounced in the adult brains. After HI, LC3-II levels increased about 2.5 times more in P60 animals than in P5 mice, comparing the ipsi- and contralateral hemispheres. The increase was even higher (more than three times) when comparing with the control brains instead of the contralateral hemispheres. Our results show for the first time that autophagy is involved in cell death after cerebral ischemia, and that the activation, as judged by the recruitment of LC3-II, was three times more pronounced in the adult brains compared with the immature brains.

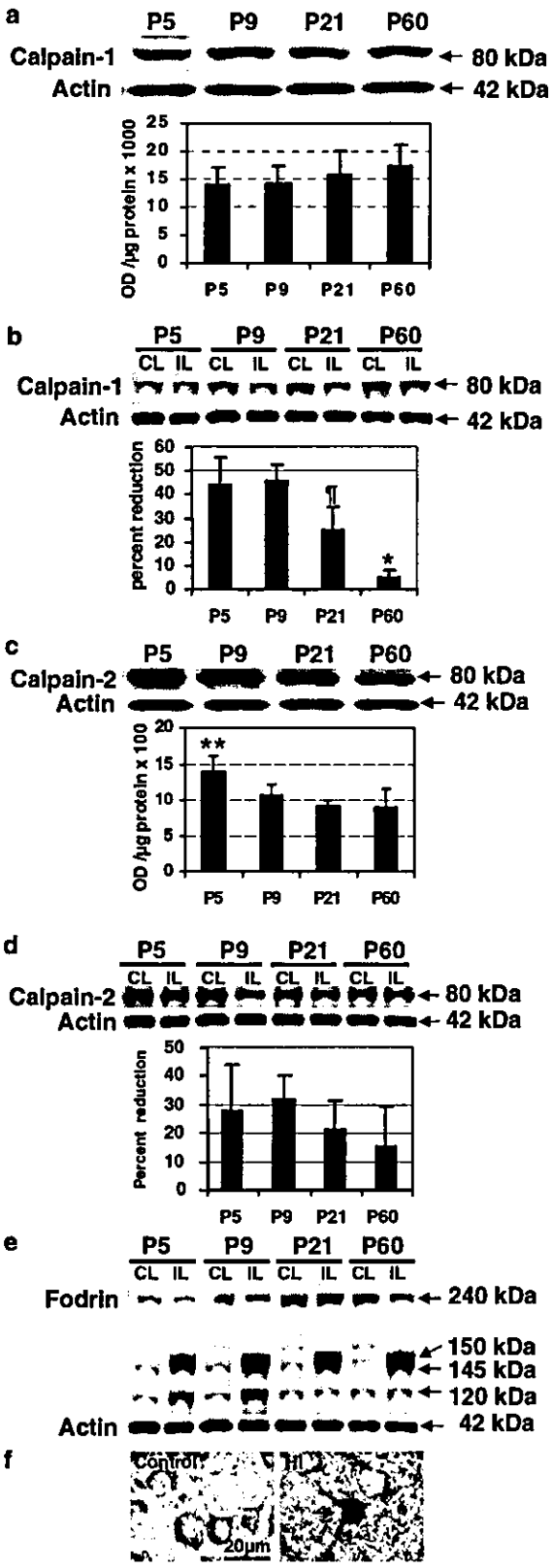

In summary, the sensitivity of neurons, and various brain regions, to injury varies with the animal's age and level of brain development. By adjusting the duration of HI in different age groups, we could produce a similar extent of overall brain damage. The most obvious developmental difference in the response to HI was that apoptotic mechanisms, both caspase-dependent and caspase-independent, were activated to a much greater extent in the immature brains compared with the juvenile and adult brains. Despite the constant levels of AIF during brain development, mitochondrial release and nuclear translocation of AIF was much more pronounced in the immature than the juvenile and adult brains. To our knowledge, this is the first report of developmental differences in AIF activation in a model of brain injury. AIF, Cyt *c* and caspase-3 are more important in the immature brain than in older animals. Calpains and NO are both important in necrotic, and to some degree, apoptotic cell death, but displayed no obvious developmental differences. Autophagy, as judged by the recruitment of LC3-II, after HI was more pronounced in the adult than in the immature brain. Taken together, our findings offer additional support for the fact that prevention and treatment of brain injury need to be adjusted to the developmental level.

Materials and Methods

Induction of HI

Unilateral HI was induced in C57/BL6 male mice on postnatal day 5 (P5), P9, P21 and P60 essentially according to the Rice–Vannucci model.[7,81] Mice were anesthetized with halothane (3.0% for induction and 1.0–1.5% for maintenance) in a mixture of nitrous oxide and oxygen (1 : 1), and the duration of anesthesia was <5 min. The left common carotid artery was cut between double ligatures of prolene sutures (6-0). After surgery, the wounds were infiltrated with a local anesthetic, and the pups were allowed to recover for 1–1.5 h. The litters were placed in a chamber perfused with a humidified gas mixture (10% oxygen in nitrogen) for 65 min (P5), 60 min (P9), 50 min (P21) or 40 min (P60). The temperature in the incubator, and the temperature of the water used to humidify the gas mixture, was kept at 36°C. After hypoxic exposure, the pups were returned to their biological

Figure 8 Calpain activation after HI. (**a**) Immunoblots of homogenates from control mice showed that the protein levels of calpain 1 (large subunit, 80 kDa) changed very little during development. (**b**) The 80 kDa large subunit was lost after HI in the ipsilateral (IL) hemispheres, compared with the contralateral (CL) hemisphere, but the reduction was more pronounced in P5 and P9 mice than that in P21 and P60 mice (*$P<0.05$ compared with P5, P9 and P21; ¶$P<0.05$ compared with P5 and P9). (**c**) Immunoblots of calpain 2 (80 kDa large subunit) in normal homogenates demonstrated a somewhat higher level in P5 brains (**$P<0.05$ compared with P21 and P60). (**d**) After HI, the 80 kDa band was partly depleted in the ipsilateral (IL) hemispheres, and the reduction was about the same at all ages. (**e**) Immunoblots of homogenate samples stained with an antibody against fodrin showed that the levels of intact, 240 kDa fodrin increased during development, as demonstrated in the contralateral (CL) hemispheres. A 150 kDa calpain-specific fodrin breakdown product (FBDP) was detected only in the ipsilateral hemispheres at 24 h post-HI. The 120 kDa caspase-3-specific breakdown product was detected only in the immature brains. The actin staining on the same membrane verified equal loading for the Western blots (**a–e**). (**f**) Representative stainings of control and postischemic (HI) tissue using an FBDP-specific antibody. An immunopositive cell is indicated by an arrow in the right panel. Bar = 20 μm

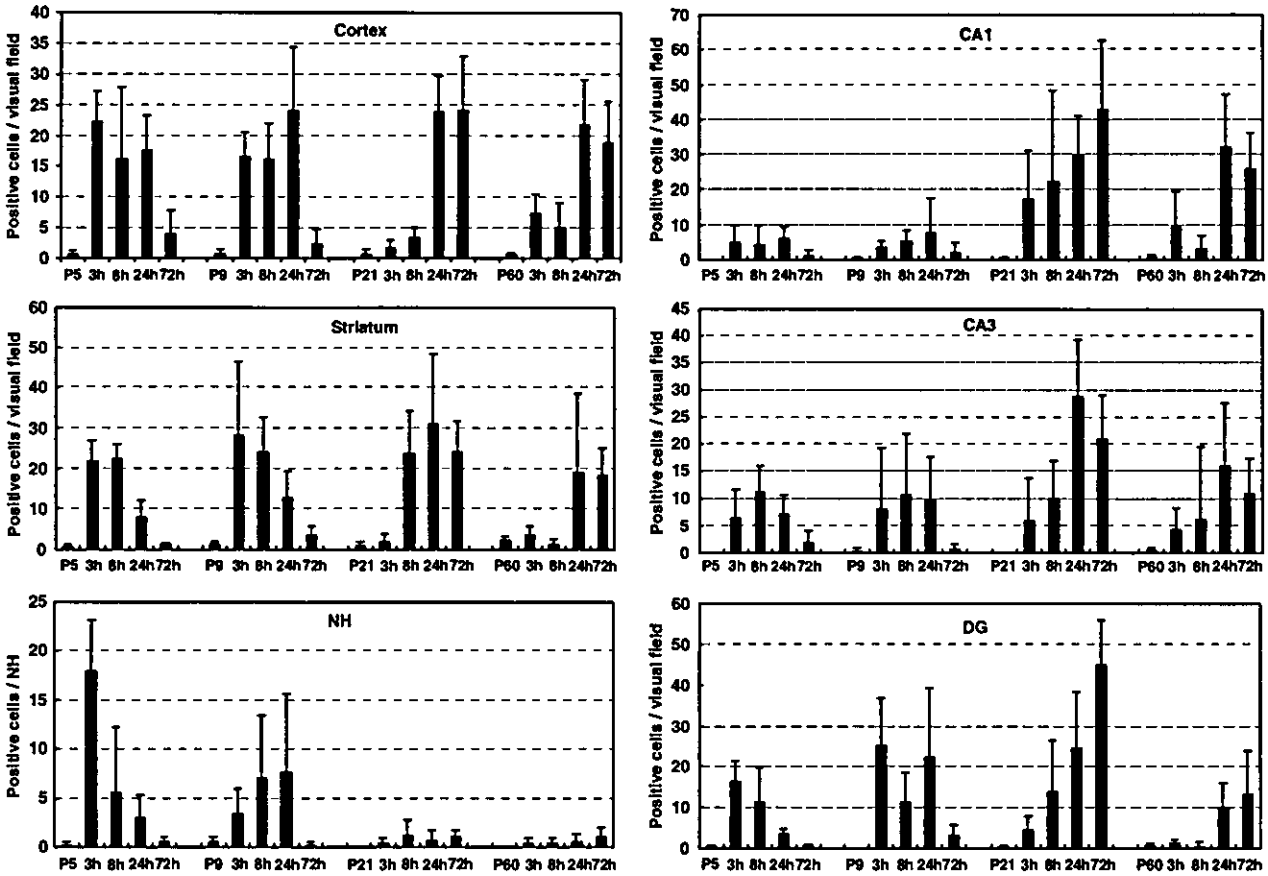

Figure 9 Counts of FBDP-positive cells in the ipsilateral hemisphere after HI. FBDP-positive cells were counted in six different regions as in Figures 3, 5 and 7. In the cortex, the number of FBDP-positive cells had increased to a high level by 3 h post-HI and decreased by 72 h after the insult in the young animals (P5, P9). For the P21 and P60 animals, however, the number of positive cells increased later, peaking by 24 h and still being elevated at 72 h post-HI. A similar pattern was seen in the striatum. Again, the lack of immunopositive cells in the NH in the P21 and P60 mice reflected the resistance to injury. The appearance of FBDP-positive cells in all the subfields of the hippocampus after HI was similar to that in the cortex, but there were more positive cells in P21 and P60 animals than in the younger P9 animals. This difference was particularly obvious in the CA1

dams and were allowed to recover for 3, 8, 24 or 72 h. The injury was evaluated at 72 h post-HI through neuropathological scoring and measurement of tissue volume loss. Control pups, subjected to neither ligation nor hypoxia, were killed at postnatal day 5, 9, 21 or 60. All animal experimentation was approved by the Ethical Committee of Göteborg (94-2003).

Sample preparation for immunoblotting and activity assay

Animals were killed by decapitation 24 h after HI ($n=5$ for each age). Control animals were killed on postnatal day 6, 10, 22 or 61 ($n=5$ for each age). The brains were rapidly dissected out on a bed of ice. Parietal cortex was dissected out by first removing the frontal and occipital poles (approx. 2–3 mm) of the brain, and second, after positioning the brain with the occipital pole face down on the dissection tray, removing the diencephalon, the medial cortex and the ventrolateral (piriform) cortex, leaving an approximately 50 mg piece of parietal cortex. This piece was dissected out from each hemisphere and 9 volumes of ice-cold homogenization buffer was added (15 mM Tris-HCl, pH 7.6, 320 mM sucrose, 1 mM dithiothretitol, 1 mM $MgCl_2$, 0.5% protease inhibitor cocktail (P8340, Sigma) and 3 mM EDTA-K). Homogenization was performed gently by hand in a 2-ml glass/glass homogenizer. Half of the homogenate was sonicated and used for Western blotting. The other half of the homogenate was centrifuged at $800 \times g$ for 10 min at 4°C. The supernatant was then centrifuged at $9200 \times g$ for 15 min at 4°C, producing a crude cytosolic fraction in the supernatant (S2), subsequently used for the caspase-3 activity assay. The pellet (P2), enriched in mitochondria, was washed, recentrifuged and used for Western blotting.

Immunohistochemistry

Mice were deeply anesthetized with 50 mg/ml phenobarbital and their brains were perfusion-fixed with 5% formaldehyde in 0.1 M phosphate buffer through the ascending aorta for 5 min. The brains were rapidly removed and immersion-fixed at 4°C for 24 h. The brains were dehydrated with xylene and graded ethanol, paraffin-embedded, serial-cut into 5 μm sections and mounted on glass slides. Antigen retrieval was performed by boiling deparaffinized sections in 10 mM sodium citrate buffer (pH 6.0) for 10 min. Nonspecific binding was blocked for 30 min with 4% horse serum

NPG.CDD.4401545

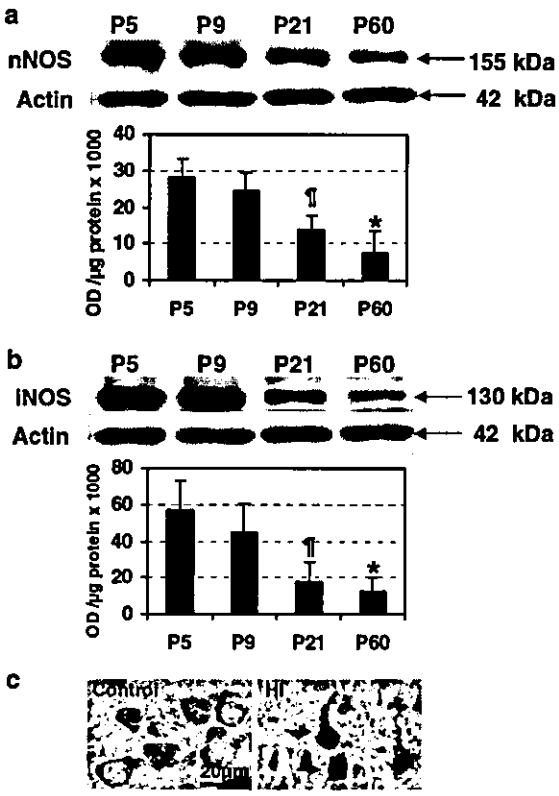

Figure 10 Developmental regulation of NOS. (**a** and **b**) Representative immunoblots of brain homogenate samples stained with an antibody against neuronal nitric oxide synthase (nNOS; 155 kDa) or inducible NOS (iNOS; 130 kDa), demonstrating a continuous decrease during development. Densitometric quantification revealed that the P5 brains had three times higher levels of nNOS and iNOS than adult ones (*$P<0.01$ and ¶$P<0.05$ compared with P5 and P9). The actin staining on the same membrane verified equal loading. (**c**) Representative stainings of control and postischemic (HI) tissue using an antibody against NOS-dependent, peroxynitrite-mediated nitrotyrosine. Two immunopositive cells are indicated by arrows in the right panel. Bar = 20 µm

(for MAP-2, Cyt *c* and AIF) or goat serum (for active caspase-3, fodrin breakdown product (FBDP) and nitrotyrosine) in phosphate-buffered saline (PBS). Anti-MAP-2 (clone HM-2, Sigma), diluted 1 : 2000 (4 µg/ml) in PBS, anti-Cyt *c* (clone 7H8.2C12, Pharmingen, San Diego, CA, USA), diluted 1 : 500 (2 µg/ml) in PBS, anti-AIF (sc-9416, from Santa Cruz Biotechnology, Santa Cruz, CA, USA), diluted 1 : 100 (2 µg/ml), antiactive caspase-3 (67342A, Pharmingen, San Diego, CA, USA), diluted 1 : 50 (10 µg/ml) in PBS, anti-FBDP[82](1 : 50) and anti-nitrotyrosine (A-21285, Molecular probes, Eugene, OR, USA), diluted 1 : 100 (10 µg/ml) in PBS were incubated for 60 min at room temperature, followed by another 60 min with a biotinylated horse anti-mouse IgG (2 µg/ml) or horse anti-goat IgG (2 µg/ml) or goat anti-rabbit IgG (2 µg/ml) diluted in PBS. Endogenous peroxidase activity was blocked with 3% H_2O_2 in PBS for 5 min. Visualization was performed using Vectastain ABC Elite with 0.5 mg/ml 3,3′-diaminobenzidine (DAB) enhanced with 15 mg/ml ammonium nickel sulfate, 2 mg/ml beta-D-glucose, 0.4 mg/ml ammonium chloride and 0.01 mg/ml beta-glucose oxidase (Sigma).

Immunoblotting

The protein concentration was determined according to Whitaker and Granum[83] adapted for microplates, using a Spectramax Plus plate reader (Molecular Devices, Sunnyvale, CA, USA). The samples were mixed with an equal volume of concentrated (3 ×) SDS-PAGE buffer and heated (96°C) for 5 min. Homogenates (50 µg protein) were run on 4–20% Tris-Glycine gels (Novex) and transferred to reinforced nitrocellulose (Schleicher & Schuell) membranes. The membranes were blocked in 30 mM Tris-HCl (pH 7.5), 100 mM NaCl and 0.1% Tween 20 (TBS-T) containing 5% fat-free milk powder for 60 min at room temperature. After washing in TBS-T, the membranes were incubated with anti-AIF (sc-9416, 1 : 1000, 0.2 µg/ml, goat polyclonal antibody, Santa Cruz, CA, USA), anti-caspase-3 (H-277, 1 : 1000, Santa Cruz, CA, USA), anti- Cyt *c* (1 : 500, clone 7H8.2C12, Pharmingen, San Diego, CA, USA), anti-calpain 1 (also called µ-calpain) (1 : 1000, 1 µg/ml, rabbit polyclonal antibody, RP1-calpain-1, Triple Point Biologics, Forest Grove, OR, USA), anti-calpain 2 (also called m-calpain) (1:1000, 1 µg/ml, rabbit polyclonal antibody, RP1-calpain-2, Triple Point Biologics, Forest Grove, OR,USA), anti-alpha-fodrin (FG6090,1 : 500, Affiniti Research Product Ltd, Mamhead, UK), anti-nNOS (clone 16, 1 : 1000, 0.25 µg/ml, BD Biosciences, San Jose, CA, USA), anti-iNOS (sc-650, 1 : 1000, 0.2 µg/ml, rabbit polyclonal antibody, Santa Cruz, CA, USA) anti-LC3 (1 : 800)[79] and anti-actin (A2066, 1 : 200, Sigma, Stockholm, Sweden) at 4°C overnight. After washing, the membranes were incubated with a peroxidase-labeled secondary antibody for 30 min at room temperature (goat anti-rabbit, 1 : 2000, horse anti-goat, 1 : 2000, or horse anti-mouse 1 : 4000). Immunoreactive species were visualized using the Super Signal Western Dura substrate (Pierce, Rockford, IL, USA) and a LAS 1000 cooled CCD camera (Fujifilm, Tokyo, Japan). Immunoreative bands were quantified using the Image Gauge software (Fujifilm, Tokyo, Japan).

Caspase activity assays

The protein concentrations were determined as above. Samples of crude cytosolic fractions (S2) (25 µl) were mixed with 75 µl of extraction buffer as described earlier.[23] Cleavage of Ac-DEVD-AMC (Peptide Institute, Osaka, Japan) was measured with an excitation wavelength of 380 nm and an emission wavelength of 460 nm, and expressed as pmol AMC released per mg protein and minute.

Injury evaluation

Neuropathological scoring

Brain injury in different regions was evaluated using a semiquantitative neuropathological scoring system as described earlier.[84] Briefly, sections were stained with thionin/acid fuchsin and scored by an observer blinded to the animals. The cortical injury was graded from 0 to 4, 0 being no observable injury and 4 confluent infarction encompassing most of the cerebral cortex. The damage in the hippocampus, striatum and thalamus was assessed both with respect to hypotrophy (shrinkage) (0–3) and observable cell injury/infraction (0–3) resulting in a neuropathological score for each brain region (0–6). The total score (0–22) was the sum of the scores for all four regions.

Tissue volume

The volumes of tissue loss were measured 3 days post-HI by sectioning the entire brains into 5 µm sections and staining every 100th section for MAP-2. The areas in the cortex, striatum, thalamus and hypothalamus

NPG.CDD.4401545

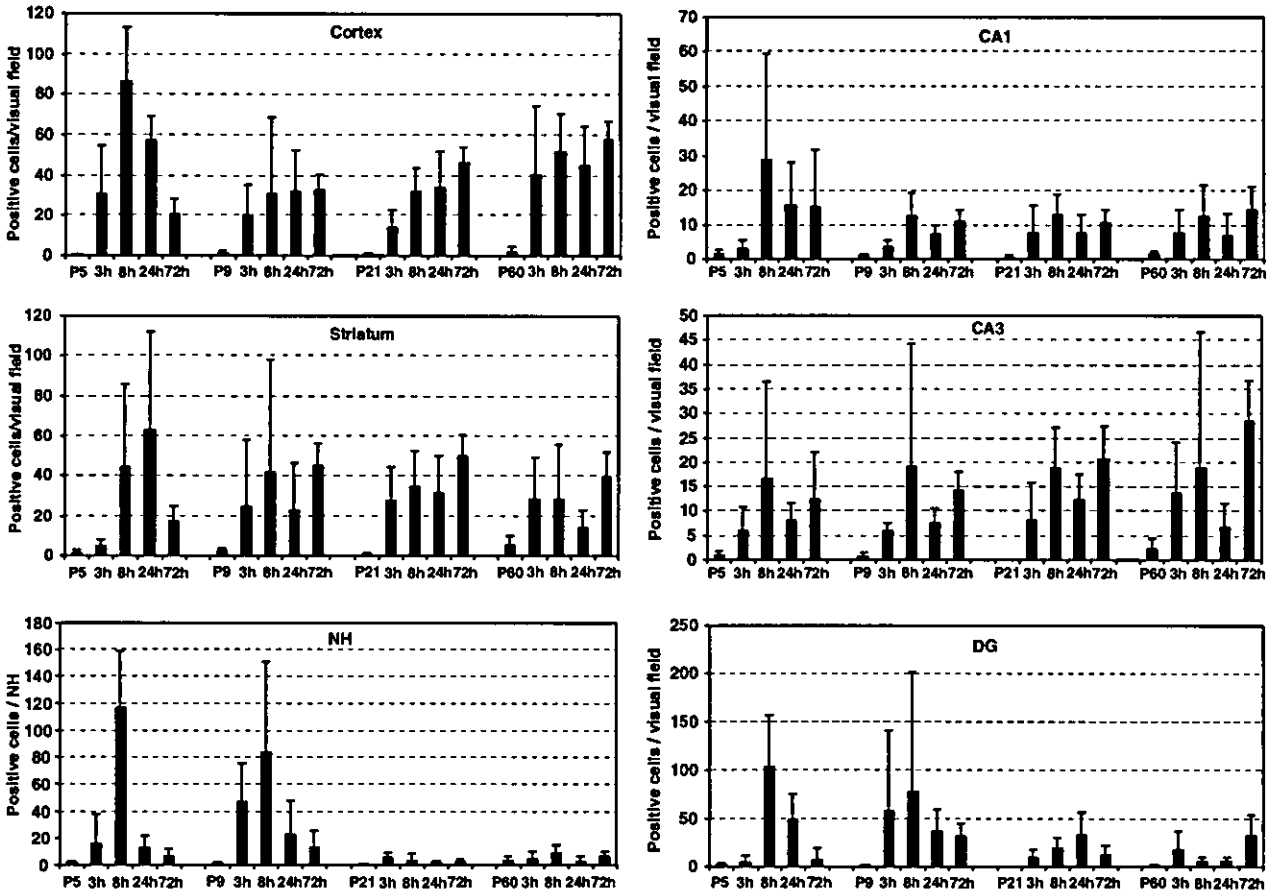

Figure 11 Counts of nitrotyrosine-positive cells in the ipsilateral hemisphere after HI. Nitrotyrosine-positive cells were counted in six different regions as in Figures 3, 5, 7 and 9. Nitrotyrosine-positive cells increased early during reperfusion and reached a peak around 8 h after HI. In P5 brains, the numbers decreased thereafter, but in P9-60 mice the numbers remained on a high level at least until 72 h post-HI. As in the case of the other injury markers, the NH did not display any nitrotyrosine-positive cells in the P21 and P60 mice, reflecting the resistance to injury at these ages. Overall, the total number of nitrotyrosine-positive cells was not so much different between the different ages except in the DG where the P5 and P9 brains displayed a higher number of immunopositive cells

displaying MAP-2 staining were measured in both hemispheres using Micro Image (Olympus, Japan) and the volumes calculated according to the Cavalieri Principle using the following formula: $V = \sum APT$, where V = total volume, $\sum A$ is the sum of the areas measured, P = the inverse of the sampling fraction and T is the section thickness.[85] The ratio of tissue loss = (contralateral volume − ipsilateral volume)/contralateral volume.

Cell counting

Cell counting was performed in the cortex, hippocampus, striatum and thalamus (NH) in the similar level for different ages (according to Bregma: −1.64 mm of P60, Franklin and Paxinos). The hippocampus was divided into the CA1, CA3 and DG subfields. Positive cells were counted at × 400 magnification (one visual field = 0.196 mm^2). In the cortex, three visual fields within an area displaying loss of MAP-2 (if any) were counted and expressed as average number per visual field. Parallel sections were used for all different staining. The counting results were corrected for possible differences in cellular density at different ages by expressing the results as number of immunopositive cells per total number of cells in the visual field or area counted.

Statistics

The Mann–Whitney U-test with Bonferroni correction, preceded by a Kruskal–Wallis test when comparing more than two groups, was used when comparing injury scores and tissue loss. ANOVA with Fisher's *post hoc* test was used when comparing quantification of Western blots and activity assay. Significance level was assigned at $P < 0.05$.

Acknowledgements

This work was supported by the Swedish Research Council (to HH and KB), the Swedish Child Cancer Foundation (Barncancerfonden) (to KB), the Göteborg Medical Society, the Åhlén Foundation, the Swedish Society of Medicine, the Wilhelm and Martina Lundgren Foundation, the Sven Jerring Foundation, the Frimurare Barnhus Foundation, the Magnus Bergvall Foundation, the National Natural Science Foundation of China (to

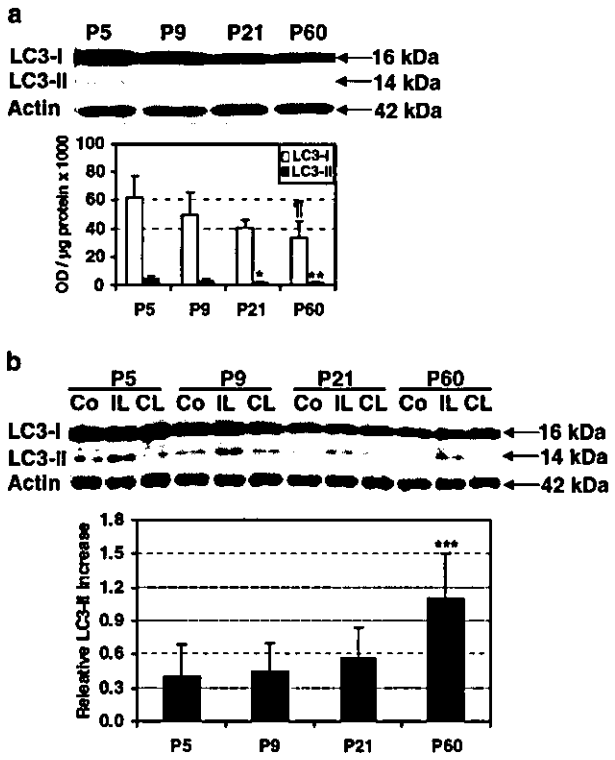

Figure 12 Immunoblot analysis of LC3-I and the autophagy marker LC3-II. (a) Representative immunoblots of normal brain homogenates demonstrating the presence of the two forms of LC3, LC3-I (16 kDa) and LC3-II (14 kDa) at all ages. The lower panel shows the results of densitometric quantification ($n=5$ per group; average $\pm$ S.D.), demonstrating that both LC3-I and LC3-II decreased approximately 50% in control brains from P5 to P60 (¶$P<0.05$, *$P<0.05$, **$P<0.01$, compared with P5). (b) The upper panel shows representative immunoblots of brain homogenates from control mice (Co), from ipsilateral hemispheres (IL) and contralateral hemispheres(CL), demonstrating an increased appearance of the LC3-II band in the ipsilateral hemispheres 24 h post-HI. The relative increase of LC3-II was calculated based on the optical density (OD) of the different bands in individual animals according to the formula: (OD of the ipsilateral – OD of the contralateral)/OD of the contralateral. LC3-II was almost three times higher in the adult (P60) brains compared with immature (P5) brains (***$P<0.0001$ compared with P5, P9 and P21). The actin staining on the same membrane verified equal loading for the Western blots

CZ, 30470598), the Bureau of Science and Technology of Henan Province, the Department of Education of Henan Province.

References

1. Hu BR, Liu CL, Ouyang Y, Blomgren K and Siesjo BK (2000) Involvement of caspase-3 in cell death after hypoxia–ischemia declines during brain maturation. J. Cereb. Blood Flow Metab. 20: 1294–1300
2. Romero AA, Gross SR, Cheng KY, Goldsmith NK and Geller HM (2003) An age-related increase in resistance to DNA damage-induced apoptotic cell death is associated with development of DNA repair mechanisms. J. Neurochem. 84: 1275–1287
3. Towfighi J, Mauger D, Vannucci RC and Vannucci SJ (1997) Influence of age on the cerebral lesions in an immature rat model of cerebral hypoxia–ischemia: a light microscopic study. Brain Res. Dev. Brain Res. 100: 149–160
4. Yager JY, Shuaib A and Thornhill J (1996) The effect of age on susceptibility to brain damage in a model of global hemispheric hypoxia–ischemia. Brain Res. Dev. Brain Res. 93: 143–154
5. Sutherland GR, Dix GA and Auer RN (1996) Effect of age in rodent models of focal and forebrain ischemia. Stroke. 27: 1663–1667; discussion 1668
6. Papadopoulos MC, Koumenis IL, Yuan TY and Giffard RG (1998) Increasing vulnerability of astrocytes to oxidative injury with age despite constant antioxidant defenses. Neuroscience. 82: 915–925
7. Rice III JE, Vannucci RC and Brierley JB (1981) The influence of immaturity on hypoxic–ischemic brain damage in the rat. Ann. Neurol. 9: 131–141
8. McDonald JW, Silverstein FS and Johnston MV (1988) Neurotoxicity of *N*-methyl-D-aspartate is markedly enhanced in developing rat central nervous system. Brain Res. 459: 200–203
9. Ikonomidou C, Mosinger JL, Salles KS, Labruyere J and Olney JW (1989) Sensitivity of the developing rat brain to hypobaric/ischemic damage parallels sensitivity to *N*-methyl-aspartate neurotoxicity. J. Neurosci. 9: 2809–2818
10. Adelson PD and Kochanek PM (1998) Head injury in children. J. Child Neurol. 13: 2–15
11. Martin LJ, Al-Abdulla NA, Brambrink AM, Kirsch JR, Sieber FE and Portera-Cailliau C (1998) Neurodegeneration in excitotoxicity, global cerebral ischemia, and target deprivation: a perspective on the contributions of apoptosis and necrosis. Brain Res. Bull. 46: 281–309
12. Northington FJ, Ferriero DM, Graham EM, Traystman RJ and Martin LJ (2001) Early neurodegeneration after hypoxia–ischemia in neonatal rat is necrosis while delayed neuronal death is apoptosis. Neurobiol. Dis. 8: 207–219
13. Yakovlev AG and Faden AI (2004) Mechanisms of neural cell death: implications for development of neuroprotective treatment strategies. NeuroRx. 1: 5–16
14. Liu CL, Siesjo BK and Hu BR (2004) Pathogenesis of hippocampal neuronal death after hypoxia–ischemia changes during brain development. Neuroscience 127: 113–123
15. Raff MC, Barres BA, Burne JF, Coles HS, Ishizaki Y and Jacobson MD (1993) Programmed cell death and the control of cell survival: lessons from the nervous system. Science 262: 695–700
16. Blomgren K, Zhu C, Wang X, Karlsson JO, Leverin AL, Bahr BA, Mallard C and Hagberg H (2001) Synergistic activation of caspase-3 by m-calpain after neonatal hypoxia–ischemia: a mechanism of 'pathological apoptosis'? J. Biol. Chem. 276: 10191–10198
17. Ota K, Yakovlev AG, Itaya A, Kameoka M, Tanaka Y and Yoshihara K (2002) Alteration of apoptotic protease-activating factor-1 (APAF-1)-dependent apoptotic pathway during development of rat brain and liver. J. Biochem. (Tokyo). 131: 131–135
18. Vekrellis K, McCarthy MJ, Watson A, Whitfield J, Rubin LL and Ham J (1997) Bax promotes neuronal cell death and is downregulated during the development of the nervous system. Development 124: 1239–1249
19. Merry DE, Veis DJ, Hickey WF and Korsmeyer SJ (1994) bcl-2 protein expression is widespread in the developing nervous system and retained in the adult PNS. Development 120: 301–311
20. Ikonomidou C, Bosch F, Miksa M, Bittigau P, Vockler J, Dikranian K, Tenkova TI, Stefovska V, Turski L and Olney JW (1999) Blockade of NMDA receptors and apoptotic neurodegeneration in the developing brain. Science 283: 70–74
21. Zhu C, Wang X, Hagberg H and Blomgren K (2000) Correlation between caspase-3 activation and three different markers of DNA damage in neonatal cerebral hypoxia–ischemia. J. Neurochem. 75: 819–829
22. Lesuisse C and Martin LJ (2002) Immature and mature cortical neurons engage different apoptotic mechanisms involving caspase-3 and the mitogen-activated protein kinase pathway. J. Cereb. Blood Flow Metab. 22: 935–950
23. Wang X, Karlsson JO, Zhu C, Bahr BA, Hagberg H and Blomgren K (2001) Caspase-3 activation after neonatal rat cerebral hypoxia–ischemia. Biol. Neonate. 79: 172–179
24. Cheng Y, Deshmukh M, D'Costa A, Demaro JA, Gidday JM, Shah A, Sun Y, Jacquin MF, Johnson EM and Holtzman DM (1998) Caspase inhibitor affords neuroprotection with delayed administration in a rat model of neonatal hypoxic–ischemic brain injury. J. Clin. Invest. 101: 1992–1999
25. Wang X, Zhu C, Hagberg H, Korhonen L, Sandberg M, Lindholm D and Blomgren K (2004) X-linked inhibitor of apoptosis (XIAP) protein protects against caspase activation and tissue loss after neonatal hypoxia–ischemia. Neurobiol. Dis. 16: 179–189

26. Kabeya Y, Mizushima N, Ueno T, Yamamoto A, Kirisako T, Noda T, Kominami E, Ohsumi Y and Yoshimori T (2000) LC3, a mammalian homologue of yeast Apg8p, is localized in autophagosome membranes after processing. EMBO J. 19: 5720–5728
27. Gill R, Soriano M, Blomgren K, Hagberg H, Wybrecht R, Miss MT, Hoefer S, Adam G, Niederhauser O, Kemp JA and Loetscher H (2002) Role of caspase-3 activation in cerebral ischemia-induced neurodegeneration in adult and neonatal brain. J. Cereb. Blood Flow Metab. 22: 420–430
28. Sidhu RS, Tuor UI and Del Bigio MR (1997) Nuclear condensation and fragmentation following cerebral hypoxia–ischemia occurs more frequently in immature than older rats. Neurosci. Lett. 223: 129–132
29. Cheng Y, Gidday JM, Yan Q, Shah AR and Holtzman DM (1997) Marked age-dependent neuroprotection by brain-derived neurotrophic factor against neonatal hypoxic–ischemic brain injury. Ann Neurol. 41: 521–529
30. Tuor UI, Chumas PD and Del Bigio MR (1995) Prevention of hypoxic–ischemic damage with dexamethasone is dependent on age and not influenced by fasting. Exp. Neurol. 132: 116–122
31. Wang X, Zhu C, Qiu L, Hagberg H, Sandberg M and Blomgren K (2003) Activation of ERK1/2 after neonatal rat cerebral hypoxia-ischaemia. J. Neurochem. 86: 351–362
32. Zhu C, Qiu L, Wang X, Hallin U, Cande C, Kroemer G, Hagberg H and Blomgren K (2003) Involvement of apoptosis-inducing factor in neuronal death after hypoxia–ischemia in the neonatal rat brain. J. Neurochem. 86: 306–317
33. Plesnila N, Zhu C, Culmsee C, Groger M, Moskowitz MA and Blomgren K (2004) Nuclear translocation of apoptosis-inducing factor after focal cerebral ischemia. J. Cereb. Blood Flow Metab. 24: 458–466
34. Fukuda H, Fukuda A, Zhu C, Korhonen L, Swanpalmer J, Hertzman S, Leist M, Lannering B, Lindholm D, Bjork-Eriksson T, Marky I and Blomgren K (2004) Irradiation-induced progenitor cell death in the developing brain is resistant to erythropoietin treatment and caspase inhibition. Cell Death Differ. 11
35. Blomgren K, Hallin U, Andersson AL, Puka-Sundvall M, Bahr BA, McRae A, Saido TC, Kawashima S and Hagberg H (1999) Calpastatin is up-regulated in response to hypoxia and is a suicide substrate to calpain after neonatal cerebral hypoxia–ischemia. J. Biol. Chem. 274: 14046–14052
36. Blomgren K, Kawashima S, Saido TC, Karlsson JO, Elmered A and Hagberg H (1995) Fodrin degradation and subcellular distribution of calpains after neonatal rat cerebral hypoxic-ischemia. Brain Res. 684: 143–149
37. Blomgren K, McRae A, Bona E, Saido TC, Karlsson JO and Hagberg H (1995) Degradation of fodrin and MAP 2 after neonatal cerebral hypoxic–ischemia. Brain Res. 684: 136–142
38. Zhu C, Wang X, Qiu L, Peeters-Scholte C, Hagberg H and Blomgren K (2004) Nitrosylation precedes caspase-3 activation and translocation of apoptosis-inducing factor in neonatal rat cerebral hypoxia-ischaemia. J. Neurochem. 90: 462–471
39. Duffy TE, Kohle SJ and Vannucci RC (1975) Carbohydrate and energy metabolism in perinatal rat brain: relation to survival in anoxia. J. Neurochem. 24: 271–276
40. Yakovlev AG, Ota K, Wang G, Movsesyan V, Bao WL, Yoshihara K and Faden AI (2001) Differential expression of apoptotic protease-activating factor-1 and caspase-3 genes and susceptibility to apoptosis during brain development and after traumatic brain injury. J. Neurosci. 21: 7439–7446
41. Wang X, Zhu C, Wang X, Gerwien JW, Schratttenholz A, Sandberg M, Leist M and Blomgren K (2004) The non-erythropoietin asialoerythropoietin protects against neonatal hypoxia–ischemia as potently as erythropoietin. J. Neurochem. (in press)
42. Hedtjarn M, Leverin AL, Eriksson K, Blomgren K, Mallard C and Hagberg H (2002) Interleukin-18 involvement in hypoxic–ischemic brain injury. J. Neurosci. 22: 5910–5919
43. Bona E, Hagberg H, Loberg EM, Bagenholm R and Thoresen M. (1998) Protective effects of moderate hypothermia after neonatal hypoxia–ischemia: short- and long-term outcome. Pediatr. Res. 43: 738–745
44. Muramatsu K, Fukuda A, Togari H, Wada Y and Nishino H (1997) Vulnerability to cerebral hypoxic–ischemic insult in neonatal but not in adult rats is in parallel with disruption of the blood–brain barrier. Stroke. 28: 2281–2288; discussion 2288–2289
45. Pohl D, Bittigau P, Ishimaru MJ, Stadthaus D, Hubner C, Olney JW, Turski L and Ikonomidou C (1999) *N*-Methyl-D-aspartate antagonists and apoptotic cell death triggered by head trauma in developing rat brain. Proc. Natl. Acad. Sci. USA. 96: 2508–2513
46. Kalou M, Rauchova H and Drahota Z (2001) Postnatal development of energy metabolism in the rat brain. Physiol. Res. 50: 315–319
47. Zhu C, Wang X, Cheng X, Qiu L, Xu F, Simbruner G and Blomgren K (2004) Post-ischemic hypothermia-induced tissue protection and diminished apoptosis after neonatal cerebral hypoxia–ischemia. Brain Res. 996: 67–75
48. Fujimura M, Morita-Fujimura Y, Kawase M, Copin JC, Calagui B, Epstein CJ and Chan PH (1999) Manganese superoxide dismutase mediates the early release of mitochondrial cytochrome *c* and subsequent DNA fragmentation after permanent focal cerebral ischemia in mice. J. Neurosci. 19: 3414–3422
49. Luetjens CM, Bui NT, Sengpiel B, Munstermann G, Poppe M, Krohn AJ, Bauerbach E, Krieglstein J and Prehn JH (2000) Delayed mitochondrial dysfunction in excitotoxic neuron death: cytochrome *c* release and a secondary increase in superoxide production. J. Neurosci. 20: 5715–5723
50. Murphy AN, Fiskum G and Beal MF (1999) Mitochondria in neurodegeneration: bioenergetic function in cell life and death. J. Cereb. Blood Flow Metab. 19: 231–245
51. Joly LM, Mucignat V, Mariani J, Plotkine M and Charriaut-Marlangue C (2004) Caspase inhibition after neonatal ischemia in the rat brain. J. Cereb. Blood Flow Metab. 24: 124–131
52. Susin SA, Lorenzo HK, Zamzami N, Marzo I, Snow BE, Brothers GM, Mangion J, Jacotot E, Costantini P, Loeffler M, Larochette N, Goodlett DR, Aebersold R, Siderovski DP, Penninger JM and Kroemer G (1999) Molecular characterization of mitochondrial apoptosis-inducing factor. Nature 397: 441–446
53. Joza N, Susin SA, Daugas E, Stanford WL, Cho SK, Li CY, Sasaki T, Elia AJ, Cheng HY, Ravagnan L, Ferri KF, Zamzami N, Wakeham A, Hakem R, Yoshida H, Kong YY, Mak TW, Zuniga-Pflucker JC, Kroemer G and Penninger JM (2001) Essential role of the mitochondrial apoptosis-inducing factor in programmed cell death. Nature 410: 549–554
54. Cao G, Clark RS, Pei W, Yin W, Zhang F, Sun FY, Graham SH and Chen J (2003) Translocation of apoptosis-inducing factor in vulnerable neurons after transient cerebral ischemia and in neuronal cultures after oxygen-glucose deprivation. J. Cereb. Blood Flow Metab. 23: 1137–1150
55. Ferrand-Drake M, Zhu C, Gido G, Hansen AJ, Karlsson JO, Bahr BA, Zamzami N, Kroemer G, Chan PH, Wieloch T and Blomgren K (2003) Cyclosporin A prevents calpain activation despite increased intracellular calcium concentrations, as well as translocation of apoptosis-inducing factor, cytochrome *c* and caspase-3 activation in neurons exposed to transient hypoglycemia. J. Neurochem. 85: 1431–1442
56. Ekdahl CT, Zhu C, Bonde S, Bahr BA, Blomgren K and Lindvall O (2003) Death mechanisms in status epilepticus-generated neurons and effects of additional seizures on their survival. Neurobiol. Dis. 14: 513–523
57. Zhang X, Chen J, Graham SH, Du L, Kochanek PM, Draviam R, Guo F, Nathaniel PD, Szabo C, Watkins SC and Clark RS (2002) Intranuclear localization of apoptosis-inducing factor (AIF) and large scale DNA fragmentation after traumatic brain injury in rats and in neuronal cultures exposed to peroxynitrite. J. Neurochem. 82: 181–191
58. Zhao H, Yenari MA, Cheng D, Barreto-Chang OL, Sapolsky RM and Steinberg GK (2004) Bcl-2 transfection via herpes simplex virus blocks apoptosis-inducing factor translocation after focal ischemia in the rat. J. Cereb. Blood Flow Metab. 24: 681–692
59. Cregan SP, Fortin A, MacLaurin JG, Callaghan SM, Cecconi F, Yu SW, Dawson TM, Dawson VL, Park DS, Kroemer G and Slack RS (2002) Apoptosis-inducing factor is involved in the regulation of caspase-independent neuronal cell death. J. Cell Biol. 158: 507–517
60. Yuan CQ, Li YN and Zhang XF (2004) Down-regulation of apoptosis-inducing factor protein by RNA interference inhibits UVA-induced cell death. Biochem. Biophys. Res. Commun. 317: 1108–1113
61. Miramar MD, Costantini P, Ravagnan L, Saraiva LM, Haouzi D, Brothers G, Penninger JM, Peleato ML, Kroemer G and Susin SA (2001) NADH oxidase activity of mitochondrial apoptosis-inducing factor. J. Biol. Chem. 276: 16391–16398
62. Klein JA, Longo-Guess CM, Rossmann MP, Seburn KL, Hurd RE, Frankel WN, Bronson RT and Ackerman SL (2002) The harlequin mouse mutation downregulates apoptosis-inducing factor. Nature 419: 367–374
63. Dutta S, Chiu YC, Probert AW and Wang KK (2002) Selective release of calpain produced alphaII-spectrin (alpha-fodrin) breakdown products by acute neuronal cell death. Biol. Chem. 383: 785–791

NPG.CDD.4401545

64. Siman R and Noszek JC (1988) Excitatory amino acids activate calpain I and induce structural protein breakdown *in vivo*. Neuron. 1: 279–287
65. Pang Z, Bondada V, Sengoku T, Siman R and Geddes JW (2003) Calpain facilitates the neuron death induced by 3-nitropropionic acid and contributes to the necrotic morphology. J. Neuropathol. Exp. Neurol. 62: 633–643
66. Saido TC, Yokota M, Nagao S, Yamaura I, Tani E, Tsuchiya T, Suzuki K and Kawashima S (1993) Spatial resolution of fodrin proteolysis in postischemic brain. J. Biol. Chem. 268: 25239–25243
67. Emgard M, Hallin U, Karlsson J, Bahr BA, Brundin P and Blomgren K (2003) Both apoptosis and necrosis occur early after intracerebral grafting of ventral mesencephalic tissue: a role for protease activation. J. Neurochem. 86: 1223–1232
68. Yamashima T, Tonchev AB, Tsukada T, Saido TC, Imajoh-Ohmi S, Momoi T and Kominami E (2003) Sustained calpain activation associated with lysosomal rupture executes necrosis of the postischemic CA1 neurons in primates. Hippocampus. 13: 791–800
69. Cai Z, Hutchins JB and Rhodes PG (1998) Intrauterine hypoxia–ischemia alters nitric oxide synthase expression and activity in fetal and neonatal rat brains. Brain Res. Dev. Brain Res. 109: 265–269
70. Higuchi Y, Hattori H, Kume T, Tsuji M, Akaike A and Furusho K (1998) Increase in nitric oxide in the hypoxic-ischemic neonatal rat brain and suppression by 7-nitroindazole and aminoguanidine. Eur. J. Pharmacol. 342: 47–49
71. Ikeno S, Nagata N, Yoshida S, Takahashi H, Kigawa J and Terakawa N (2000) Immature brain injury via peroxynitrite production induced by inducible nitric oxide synthase after hypoxia–ischemia in rats. J. Obstet. Gynaecol. Res. 26: 227–234
72. Peeters-Scholte C, Koster J, van den Tweel E, Blomgren K, Hamers N, Zhu C, van Buul-Offers S, Hagberg H, van Bel F, Heijnen C and Groenendaal F (2002) Effects of selective nitric oxide synthase inhibition on IGF-1, caspases and cytokines in a newborn piglet model of perinatal hypoxia–ischaemia. Dev. Neurosci. 24: 396–404
73. Andersen JK (2004) Oxidative stress in neurodegeneration: cause or consequence? Nat. Med. 10 (Suppl): S18–S25
74. McQuillen PS and Ferriero DM (2004) Selective vulnerability in the developing central nervous system. Pediatr. Neurol. 30: 227–235
75. Bursch W (2001) The autophagosomal-lysosomal compartment in programmed cell death. Cell Death Differ. 8: 569–581
76. Xue L, Fletcher GC and Tolkovsky AM (1999) Autophagy is activated by apoptotic signalling in sympathetic neurons: an alternative mechanism of death execution. Mol. Cell Neurosci. 14: 180–198
77. Kabeya Y, Mizushima N, Yamamoto A, Oshitani-Okamoto S, Ohsumi Y and Yoshimori T (2004) LC3, GABARAP and GATE16 localize to autophagosomal membrane depending on form-II formation. J. Cell Sci. 117 (Part 13): 2805–2812
78. Asanuma K, Tanida I, Shirato I, Ueno T, Takahara H, Nishitani T, Kominami E and Tomino Y (2003) MAP-LC3, a promising autophagosomal marker, is processed during the differentiation and recovery of podocytes from PAN nephrosis. FASEB J. 17: 1165–1167
79. Yu WH, Kumar A, Peterhoff C, Shapiro Kulnane L, Uchiyama Y, Lamb BT, Cuervo AM and Nixon RA (2004) Autophagic vacuoles are enriched in amyloid precursor protein-secretase activities: implications for beta-amyloid peptide over-production and localization in Alzheimer's disease. Int. J. Biochem. Cell Biol. 36: 2531–2540
80. Puka-Sundvall M, Gajkowska B, Cholewinski M, Blomgren K, Lazarewicz JW and Hagberg H (2000) Subcellular distribution of calcium and ultrastructural changes after cerebral hypoxia–ischemia in immature rats. Brain Res. Dev. Brain Res. 125: 31–41
81. Sheldon RA, Sedik C and Ferriero DM (1998) Strain-related brain injury in neonatal mice subjected to hypoxia–ischemia. Brain Res. 810: 114–122
82. Bahr BA, Tiriveedhi S, Park GY and Lynch G (1995) Induction of calpain-mediated spectrin fragments by pathogenic treatments in long-term hippocampal slices. J. Pharmacol. Exp. Ther. 273: 902–908
83. Whitaker JR and Granum PE (1980) An absolute method for protein determination based on difference in absorbance at 235 and 280 nm. Anal. Biochem. 109: 156–159
84. Hagberg H, Wilson MA, Matsushita H, Zhu C, Lange M, Gustavsson M, Poitras MF, Dawson TM, Dawson VL, Northington F and Johnston MV (2004) PARP-1 gene disruption in mice preferentially protects males from perinatal brain injury. J. Neurochem. 90: 1068–1075
85. Mallard EC, Williams CE, Gunn AJ, Gunning MI and Gluckman PD (1993) Frequent episodes of brief ischemia sensitize the fetal sheep brain to neuronal loss and induce striatal injury. Pediatr. Res. 33: 61–65

NPG.CDD.4401545

Available online at www.sciencedirect.com
SCIENCE DIRECT
Journal of Chemical Neuroanatomy 28 (2004) 101–105
Journal of CHEMICAL NEUROANATOMY
www.elsevier.com/locate/jchemneu

Review

Caspases involved in ER stress-mediated cell death

Takashi Momoi*

Divisions of Development and Differentiation, National Institute of Neuroscience, NCNP, 4-1-1 Ogawahigashi-machi, Kodaira, Tokyo 187-8502, Japan

Received 9 August 2003; received in revised form 11 May 2004; accepted 11 May 2004
Available online 28 July 2004

Abstract

Caspases are cysteine proteases involved in apoptotic pathways. Excess endoplasmic reticulum (ER) stress, induced by the accumulation of unfolded or malfolded proteins, activates various apoptotic pathways. Crosstalk between the mitochondria and ER plays an essential role in ER stress-mediated cell death. The cytochrome *c*-dependent apoptotic pathway is activated by ER stress. On the other hand, caspase-12, which is located at the ER, is also activated by excess ER stress and results in cell death in the absence of the cytochrome *c*-dependent pathway. The predominant apoptotic pathway may differ among cell type and differentiation stage.

Keywords: Endoplasmic reticulum; Unfolded protein response; Apoptosis

1. Cell death and caspase activation

Caspases, a family of cysteine proteases which have the consensus sequence QACXG in the active site, are critical mediators of programmed cell death. Thus far, 14 family members have been identified (Cryns and Yuan, 1998). Caspases are activated by other caspase family members in a sequential cascade of cleavage. Two major apoptotic pathways have been identified. One involves caspase-8, which has a death effector domain (DED) at the N-terminus, and mediates signals downstream of death receptors located on the plasma membrane (Boldin et al., 1996). Caspase-8 is recruited to a death-inducing stimulating complex (DISC) and then activated (Kischkel et al., 1995; Muzio et al., 1996). The other involves caspase-9, which has a caspase-associated recruit domain (CARD) in the N-terminus and is known to mediate apoptotic signals after mitochondrial damage. Cytochrome *c* release from mitochondria plays a key role in caspase-9-mediated apoptosis. Caspase-9 is activated in an apoptosome complex by associating with Apaf-1, which is bound to cytochrome *c*, via the CARD domain (Zou et al., 1997, 1999).

Members of the Bcl-2 family dually regulate cytochrome *c* release from mitochondria (Thornberry and Lazebnik, 1998). Bax and Bad positively regulate release, while Bcl-2 and Bcl-xL negatively regulate it. Bid, BH3-only Bcl-2 protein, is a protein known to interact with both Bcl-2 and Bax through its BH3 domain (Wang et al., 1996). Caspase-8 processes Bid, and the C-terminal part of Bid then translocates to the mitochondrial membrane and triggers cytochrome *c* release (Li et al., 1998; Luo et al., 1998). Thus, the mitochondria are centers for the regulation of cell death.

2. ER stress and cell death

The endoplasmic reticulum (ER) is the site of assembly of polypeptide chains destined for secretion or routing into various subcellular compartments. When cells are exposed to ER stresses caused by agents such as tunicamycin (a specific inhibitor of N-glycosylation in the ER), brefeldin A (an inhibitor of ER/Golgi transport) or thapsigargin (an inhibitor of Ca^{2+}-ATPase), malfolded or unfolded proteins accumulate in the ER lumen (Kaufman, 1999). Cells respond to these stresses by increasing the transcription of genes encoding ER molecular chaperons, including that for the glucose regulated protein GRP78 (Bip), a chaperone which increases protein folding in the ER lumen. This cellular response is

* Tel.: +81 423 41 2711; fax: +81 42 346 1751.
E-mail address: momoi@ncnp.go.jp (T. Momoi).

0891-0618/$ – see front matter © 2004 Elsevier B.V. All rights reserved.
doi:10.1016/j.jchemneu.2004.05.008

known as the unfolded protein response (UPR) and occurs via the ER stress sensor protein IRE1α.

Recently, the ER was shown to be another center of regulation for cell death (Ferri and Kroemer, 2001). Excess amounts of malfolded and unfolded proteins are translocated from the ER to the cytoplasm and are degraded by a ubiquitine-proteasome system called the ER-associated degradation system (ERAD). However, if degradation is not sufficient, prolonged stress activates various apoptotic pathways. IRE1α can recruit the cytosolic adaptor protein, TNF receptor-associated factor 2 (TRAF2), which in turn recruits and activates ASK, the proximal component of the c-Jun N-terminal kinase (JNK) pathway (Kyriakis et al., 1994; Urano et al., 2000). Prolonged activation of ASK and JNK results in apoptosis (Tournier et al., 2000) (Fig. 1).

The downstream apoptotic pathway of ER stress-mediated cell death has recently been studied in more detail. JNK is translocated to the mitochondrial membrane (Aoki et al., 2002) and it stimulates the phosphorylation of Bim, BH3-only Bcl-2 protein (Lei and Davis, 2003; Putcha et al., 2003), which in turn are critical for Bax-dependent cytochrome *c* release. A Bcl-2 protein targeted to the ER, Bcl-2/cb5, inhibits ER stress-mediated cytochrome *c* release (Häcki et al., 2000). In contrast, RTN-xs, a member of the reticulon (RTN) family, reduces the anti-apoptotic activities of Bcl-2 and Bcl-xL in tunicamycin-induced cell death by interacting with them at the ER (Tagami et al., 2000). Thus, the signaling pathway mediated by cytochrome *c* release plays an essential role in ER stress-mediated apoptosis. In addition to cytochrome *c* release from the mitochondria, excess ER stress induces caspase-12 activation. However, their relationship has not been clearly understood.

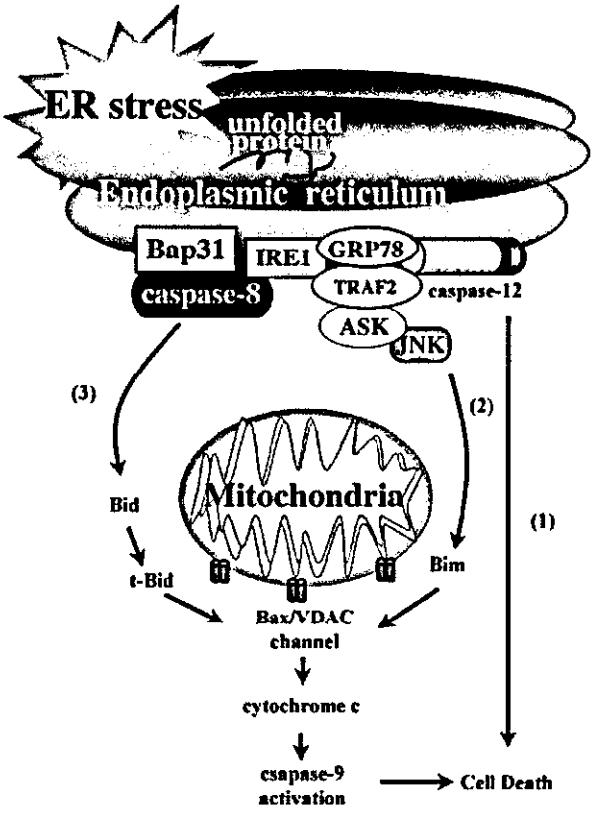

Fig. 1. ER stress-mediated apoptotic pathways in various mouse cells. Three major apoptotic pathways have been reported in the ER stress-mediated cell death: (1) caspase-12-dependent apoptotic pathway; (2) ASK/JNK pathway, which induces cytochrome *c* release from mitochondria and caspase-9 activation; (3) Bap31 and caspase-8 pathway, which also induces cytochrome *c* release from mitochondria and caspase-9 activation.

3. Activation of caspase-12

Caspase-12 (Van de Craen et al., 1997) is specifically localized on the cytoplasmic side (outer membrane) of the ER and is thought to play a role in ER stress-mediated cell death (Nakagawa et al., 2000). Caspase-12 is activated by ER stress stimuli such as tunicamycin, brefeldin A, and thapsigargin, but not by membrane- or mitochondrial-targeted apoptotic signals. ER stress-mediated apoptosis is partly suppressed by a *caspase-12* deficiency, suggesting involvement of the caspase-12 in this apoptosis.

Caspase-12, like most other members of the caspase family, requires cleavage of the prodomain to activate its proapoptotic form. So far, several possible molecular mechanisms for the processing of caspase-12 have been postulated (Fig. 2). Nakagawa and Yuan (2000) reported

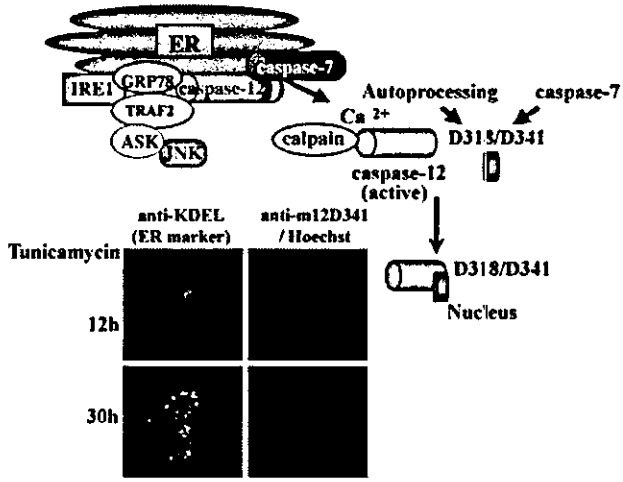

Fig. 2. Processing of caspase-12 by ER stress. Upon ER stress, caspase-12 is associated with caspase-7 and processed at D^{94} and D^{341} by caspase-7 (Rao et al., 2001). Calpain, calcium-activated cytein protease, also cleaves N-terminal site and then caspase-12 is autoprocessed at D^{318} (Nakagawa and Yuan, 2000). By immunostaining using anti-m12D341, antibody specifically reacting with the processed fragment of caspase-12 at D^{341}, Fujita et al. (2002) demonstrated that active form of caspase-12 is translocated from ER to nucleus. Anti-m12D341 immunoreactivity is detected in the ER at 12 h but also in the nucleus at 30 h after tunicamycin (1 μM) treatment. Red; anti-m12D341 , green; anti-KDEL (ER marker), blue; Hoechst 33342.

that m-calpain, another cysteine protease, is responsible for cleaving procaspase-12 to generate the active caspase-12. Caspase-12 is initially processed at the N-terminal region by calpain, activated by ER stress. Caspase-12 is then activated and autoprocessed at D^{318}. Thus, calcium released from the ER may trigger a novel apoptotic pathway involving calcium-mediated calpain activation and crosstalk between the calpain and caspase families.

Caspase-12 possesses a CARD domain (Fig. 3) (Lamkanfi et al., 2002), through which caspase-9 and Apaf-1 interact and form apoptosome complexes. It may be possible that, like caspase-9, caspase-12 is activated by its association with an Apaf-1-like protein. However, while *apaf-1* (−/−) fibroblasts are resistant to apoptotic insults that induce the intrinsic apoptotic pathway, these cells are susceptible to apoptosis induced by thapsigargin and brefeldin A (Rao et al., 2002a). Caspase-12 may bind to molecules other than Apaf-1.

GRP78 is involved in polypeptide translocation across the ER membrane, and also acts as an apoptotic regulator by protecting the host cell against ER stress-induced cell death. Treatment of cells with ER stress inducers such as brefeldin A and thapsigargin causes GRP78 to redistribute from the ER lumens, so that subpopulations exist in the cytosol and as ER transmembrane protein (Rao et al., 2002b; Reddy et al., 2003) and induces the expression of the caspase-12 protein and also leads to the translocation of cytosolic caspase-7 to the ER surface. GRP78 forms a complex with caspase-7 and caspase-12 and prevents the release of caspase-12 from the ER, but upon excess ER stress, caspase-7 associates with caspase-12 and cleaves the prodomain at D^{94} to initiate the processing of caspase-12 at D^{341}, resulting in increased cell death (Rao et al., 2001) (Fig. 2).

The other molecule which complexes with caspase-12 is TRAF-2. Caspase-12 is shown to be released from TRAF2 complexes by ER stress and is then autoprocessed via homodimerization (Yoneda et al., 2001). In that study c-Jun N-terminal inhibitory kinase (JIK) is identified as a binding partner of IRE1α. JIK modulates IRE1α-TRAF2 complex formation and the resultant alteration to JNK signaling from IRE1α. In response to ER stress, TRAF2 plays crucial roles, not only in the signaling of the JNK pathway but also in the activation of caspase-12, to transduce signals from IRE1α. Thus, TRAF-2 is a missing link in the ER stress-induced apoptosis signaling pathway, one which connects the stress sensor molecule IRE1α and the activation of caspase-12.

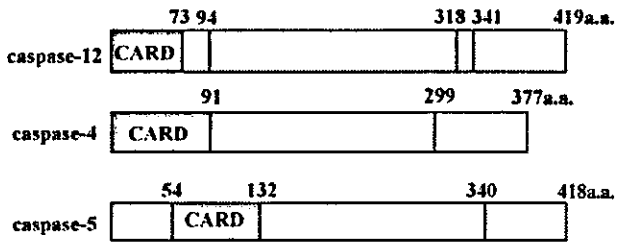

Fig. 3. Molecular structure of mouse casapse-12, human caspase-4 and caspase-5. Amino acid sequences of mouse caspase-12 (Van de Craen et al., 1997) are 48 and 45% identical to those of human caspase-4 and caspase-5 (Faucheu et al., 1995; Kamens et al., 1995; Munday et al., 1995), respectively. Mouse caspase-12 has putative cleavage sites at D^{318}(ATAD^{318}) and D^{341}(VETD^{341}), while caspase-4 and caspase-5 have their cleavage sites at D^{299}(VEKD^{299}) and D^{340}(EEKD^{340}), respectively. The tetrapeptide at cleavage site of capase-4 at D^{299} is very similar to that of caspase-12 at D^{341}. Caspase-12, caspase-4 and caspase-5 have CARD domain at their N-terminal regions, 4–73, 2–91, and 54–132, respectively.

4. Cytochrome *c*-independent apoptotic pathway via caspase-12 activation

Although activation of caspase-12 from procaspase-12 is specifically induced following insult to the ER, the functional consequences of caspase-12 activation have remained unclear. In a cell free-system, ER stress activates a mitochondrial and Apaf-1-independent, intrinsic apoptotic pathway (Rao, 2002a). Caspase-12 activates caspase-9 without the involvement of cytochrome *c* (Morishima et al., 2002). It may be possible that procaspase-9 is a substrate of caspase-12 and that ER stress triggers a specific cascade involving caspases-12, -9, and -3 in a cytochrome *c*-independent manner in vivo.

Fujita et al. (2002) prepared antisera against the putative caspase-12 cleavage sites, D^{318} and D^{341}, (anti-m12D318 and anti-m12D341) and examined the localization of the processed fragments of caspase-12 following induction by tunicamycin. Anti-m12D318 and anti-m12D341 immunoreactivity sites are located not only in the ER but also around and within the nuclei of the apoptotic cells. Processing at the N-terminal region is necessary for the release of the protein from the ER and for the translocation of the processed caspase-12 into the nuclei. Activated caspase-12 may directly participate in apoptotic events in the nuclei.

5. Human caspase-12

In contrast to mouse, functional caspase-12 is lacking in humans (Fischer et al., 2002). Alignment of the murine caspase-12 cDNA with the human genome sequence indicates that the human *caspase-12* gene is localized at a single locus within the caspase-1/ICE gene cluster including caspase-1, caspase-4, and caspase-5 on chromosome 11q22.3. The human *caspase-12* gene has nine alternatively splice transcripts, but a frame shift mutation and a premature stop codon, which are present in all splice variants, preclude the expression of a full length protein. An additional loss-of-function mutation within the SHG box, a critical site in caspases, prohibits any proteins, if any are produced, from acting catalytically.

In place of caspase-12, other caspases may play roles in the ER stress-mediated cell death of human cells. Candidate caspases involved are caspase-4 and caspase-5. Procaspase-4 and procaspase-5 amino acid sequences are 59 and 54%

identical to mouse procaspase-11, respectively. Procaspase-4 and procaspase-5 have an amino acid sequence identity of 77% (the next highest identity score being 55% between procaspase-1 and procaspase-4) and are localized at the locus of 11q22.3. On the basis of these results, human caspase-4 and caspase-5 are considered to be duplicated counterparts of mouse caspase-11 (Lamkanfi et al., 2002).

However, both caspase-4 and caspase-5 have a CARD domain at the N-terminal and also show high similarity to mouse caspase-12 (Fig. 3) (Faucheu et al., 1995; Kamens et al., 1995; Munday et al., 1995); i.e. procaspase-4 and procaspase-5 amino acid sequences are 48 and 45% identical to procaspase-12, respectively. Furthermore, the tetrapeptide around the cleavage site of caspase-12, $VETD^{341}$, is similar to that of human caspase-4, $VEKD^{299}$. Very recently, it has been shown that caspase-4 is located at the ER and activated by ER stress (Hitomi et al., 2004). Thus, caspase-4 is involved in the ER stress-mediated cell death of human cells. At present, however, it is not clear whether caspase-4 and caspase-12 are associated with same molecules located at ER via their CARD domain and activated by the common molecular mechanism.

6. Cytochrome *c*dependent apoptotic pathway activation by ER stress

The level of expression of caspase-12 is different in various mouse cells (Kalai et al., 2003; Fujita et al., unpublished observation). In C2C12 cells, mouse myoblasts, the level of caspase-12 is high and mainly activated by ER stress. In contrast, in P19 embryonal carcinoma (P19 EC) cells, the level of caspase-12 is very low and ER stress induces cytochrome *c*/caspase-9 activation, without involving caspase-12 (Jimbo et al., 2003). Caspase-12 may not be a predominant apoptotic pathway activated by ER stress in some types of cells. The predominant apoptotic pathway may differ among cell type and differentiation stage.

Caspase-8 deficiency inhibits the cytochrome *c* release and Bid processing induced by ER stress (Jimbo et al., 2003). Thus, in parallel with caspase-12 activation and ASK/JNK activation, ER stress independently triggers caspase-8 activation, resulting in cytochrome *c*/caspase-9 activation via Bid processing (Fig. 1). In addition to ASK/JNK, the processed Bid (tBid) plays a role in the ER-mitochondria crosstalk during ER stress-mediated cell death.

Another molecule mediating ER-mitochondria crosstalk is the caspase-8 cleavage fragment of BAP31, an integral membrane protein of ER (Annaert et al., 1997). BAP31 is one of a limited number of substrates for caspase-8. A caspase-resistant BAP31 mutant inhibited several features of Fas-induced apoptosis, including the release of cytochrome *c* from mitochondria (Nguyen et al., 2000). BAP31 interacts with a unique isoform of caspase-8 (Breckenridge et al., 2002). ER stress may induce the BAP31 and caspase-8 complex and activate caspase-8. A p20 caspase cleavage fragment of BAP31 causes the early release of Ca^{2+} from the ER, the concomitant uptake of Ca^{2+} into mitochondria, and the mitochondrial recruitment of Drp1. Drp1 is a dynamin-related protein that mediates the scission of the outer mitochondrial membrane, resulting in dramatic fragmentation and fission of the mitochondrial network (Breckenridge et al., 2003). Caspase-8 cleavage of BAP31 at the ER may also stimulate Ca^{2+}-dependent mitochondrial fission, enhancing the release of cytochrome *c* from the mitochondria. Cytochrome *c*-dependent apoptotic pathway activated by ER–mitochondria crosstalk seems to play an essential role in the ER stress-mediated cell death.

7. In conclusion

Excess ER stress induces the activation of various apoptotic pathways, and the predominant apoptotic pathway may differ among cell types. The ER stress-mediated apoptotic pathways have been discussed as follows:

1. ASK/JNK is activated, resulting in cytochrome *c*-mediated cell death.
2. Caspase-8 is also activated by its interaction with BAP31, resulting in cytochrome *c*-mediated cell death.
3. Caspase-12 is activated via processing by calpain or caspase-7, resulting in cytochrome *c*-independent cell death.

Acknowledgements

I thank Drs. E. Fujita, and Y. Kouroku, for their valuable discussion during preparation of the manuscript.

References

Aoki, H., Kang, P.M., Hampe, J., Yoshimura, K., Noma, T., Matsuzaki, M., Izumo, S., 2002. Direct activation of mitochondrial apoptosis machinery by c-Jun N-terminal kinase in adult cardiac myocytes. J. Biol. Chem. 277, 10244–10250.

Annaert, W.G., Becker, B., Kistner, U., Reth, M., Jahn, R., 1997. Export of cellubrevin from the endoplasmic reticulum is controlled by BAP31. J. Cell Biol. 139, 1397–1410.

Breckenridge, D.G., Nguyen, M., Kuppig, S., Reth, M., Shore, G.C., 2002. The procaspase-8 isoform, procaspase-8L, recruited to the BAP31 complex at the endoplasmic reticulum. Proc. Natl. Acad. Sci. U.S.A. 99, 4331–4336.

Breckenridge, D.G., Stojanovic, M., Marcellus, R.C., Shore, G.C., 2003. Caspase cleavage product of BAP31 induces mitochondrial fission through endoplasmic reticulum calcium signals, enhancing cytochrome *c* release to the cytosol. J. Cell Biol. 160, 1115–1127.

Boldin, M.P., Goncharov, T.M., Goltsev, Y.V., Wallach, D., 1996. Involvement of MACH, a novel MORT1/FADD-interacting protease, in Fas/APO-1- and TNF receptor-induced cell death. Cell 85, 803–815.

Cryns, V., Yuan, J., 1998. Proteases to die for. Genes Dev. 12, 1551–1572.

Faucheu, C., Diu, A., Chan, A.W., Blanchet, A.M., Miossec, C., Herve, F., Collard-Dutilleul, V., Gu, Y., Aldape, R.A., Lippke, J.A., 1995. A novel human protease similar to the interleukin-1 beta converting

enzyme induces apoptosis in transfected cells. EMBO J. 14, 1914–1922.

Ferri, K.F., Kroemer, G., 2001. Organelle-specific initiation of cell death pathways. Nat. Cell Biol. 3, 255–263.

Fischer, H., Koenig, U., Eckhart, L., Tschachler, E., 2002. Human caspase 12 has acquired deleterious mutations. Biochem. Biophys. Res. Commun. 293, 722–726.

Fujita, E., Kouroku, Y., Jimbo, A., Isoai, A., Maruyama, K., Momoi, T., 2002. Caspase-12 processing and fragment translocation into nuclei of tunicamycin-treated cells. Cell Death Differ. 9, 1108–1114.

Häcki, J., Egger, L., Monney, L., Conus, S., Rosse, T., Fellay, I., Borner, C., 2000. Apoptotic crosstalk between the endoplasmic reticulum and mitochondria controlled by Bcl-2. Oncogene 19, 2286–2295.

Hitomi, J., Katayama, T., Eguchi, Y., Kudo, T., Taniguchi, M., Koyama, Y., Manabe, T., Yamagishi, S., Bando, Y., Imaizumi, K., Tsujimoto, Y., Tohyama, M., 2004. Involvement of caspase-4 in endoplasmic reticulum stress-induced apoptosis and A{beta}-induced cell death. J Cell Biol. 165, 347–356.

Jimbo, A., Fujita, E., Kouroku, Y., Ohnishi, J., Inohara, N., Kuida, K., Sakamaki, K., Yonehara, S., Momoi, T., 2003. ER stress induces caspase-8 activation, stimulating cytochrome *c* release and caspase-9 activation. Exp. Cell Res. 283, 156–166.

Kalai, M., Lamkanfi, M., Denecker, G., Boogmans, M., Lippens, S., Meeus, A., Declercq, W., Vandenabeele, P., 2003. Regulation of the expression and processing of caspase-12. J. Cell Biol. 162, 457–467.

Kamens, J., Paskind, M., Hugunin, M., Talanian, R.V., Allen, H., Banach, D., Bump, N., Hackett, M., Johnston, C.G., Li, P., 1995. Identification and characterization of ICH-2, a novel member of the interleukin-1 beta-converting enzyme family of cysteine proteases. J. Biol. Chem. 23, 15250–15256.

Kaufman, R.J., 1999. Stress signaling from the lumen of the endoplasmic reticulum: coordination of gene transcriptional and translational controls. Genes Dev. 13, 1211–1233.

Kischkel, F.C., Hellbardt, S., Behrmann, I., Germer, M., Pawlita, M., Krammer, P.H., Peter, M.E., 1995. Cytotoxicity-dependent APO-1 (Fas/CD95)-associated proteins form a death-inducing signaling complex (DISC) with the receptor. EMBO J. 14, 5579–5588.

Kyriakis, J.M., Banerjee, P., Nikolakaki, E., Dai, T., Rubie, E.A., Ahmad, M.F., Avruch, J., Woodgett, J.R., 1994. The stress-activated protein kinase subfamily of c-Jun kinases. Nature 369, 156–160.

Lamkanfi, M., Declercq, W., Kalai, M., Saelens, X., Vandenabeele, P., 2002. Alice in caspase land. A phylogenetic analysis of caspases from worm to man. Cell Death Differ. 9, 358–361.

Lei, K., Davis, R.J., 2003. JNK phosphorylation of Bim-related members of the Bcl2 family induces Bax-dependent apoptosis. Proc. Natl. Acad. Sci. U.S.A. 4, 2432–2437.

Li, H., Zhu, H., Xu, C.J., Yuan, J., 1998. Cleavage of BID by caspase 8 mediates the mitochondrial damage in the Fas pathway of apoptosis. Cell 94, 491–501.

Luo, X., Budihardjo, I., Zou, H., Slaughter, C., Wang, X., 1998. Bid, a Bcl2 interacting protein, mediates cytochrome *c* release from mitochondria in response to activation of cell surface death receptors. Cell 94, 481–490.

Morishima, N., Nakanishi, K., Takenouchi, H., Shibata, T., Yasuhiko, Y., 2002. An endoplasmic reticulum stress-specific caspase cascade in apoptosis. Cytochrome *c*-independent activation of caspase-9 by caspase-12. J. Biol. Chem. 277, 34287–34294.

Munday, N.A., Vaillancourt, J.P., Ali, A., Casano, F.J., Miller, D.K., Molineaux, S.M., Yamin, T.T., Yu, V.L., Nicholson, D.W., 1995. Molecular cloning and pro-apoptotic activity of ICErelII and ICErelIII, members of the ICE/CED-3 family of cysteine proteases. J. Biol. Chem. 270, 15870–15876.

Muzio, M., Chinnaiyan, A.M., Kischkel, F.C., O'Rourke, K., Shevchenko, A., Ni, J., Scaffidi, C., Bretz, J.D., Zhang, M., Gentz, R., Mann, M., Krammer, P.H., Peter, M.E., Dixit, V.M., 1996. FLICE, a novel FADD-homologous ICE/CED-3-like protease, is recruited to the CD95 (Fas/APO-1) death-inducing signaling complex. Cell 85, 817–827.

Nakagawa, T., Yuan, J., 2000. Cross-talk between two cysteine protease families. Activation of caspase-12 by calpain in apoptosis. J. Cell Biol. 150, 887–894.

Nakagawa, T., Zhu, H., Morishima, N., Li, E., Xu, J., Yankner, B.A., Yuan, J., 2000. Caspase-12 mediates endoplasmic-reticulum-specific apoptosis and cytotoxicity by amyloid-beta. Nature 403, 98–103.

Nguyen, M., Breckenridge, D.G., Ducret, A., Shore, G.C., 2000. Caspase-resistant BAP31 inhibits fas-mediated apoptotic membrane fragmentation and release of cytochrome *c* from mitochondria. Mol. Cell Biol. 20, 6731–6740.

Putcha, G.V., Le, S., Frank, S., Besirli, C.G., Clark, K., Chu, B., Alix, S., Youle, R.J., LaMarche, A., Maroney, A.C., Johnson Jr., E.M., 2003. JNK-mediated BIM phosphorylation potentiates BAX-dependent apoptosis. Neuron 38, 899–914.

Rao, R.V., Hermel, E., Castro-Obregon, S., del Rio, G., Ellerby, L.M., Ellerby, H.M., Bredesen, D.E., 2001. Coupling endoplasmic reticulum stress to the cell death program. Mechanism of caspase activation. J. Biol. Chem. 276, 33869–33874.

Rao, R.V., Castro-Obregon, S., Frankowski, H., Schuler, M., Stoka, V., del Rio, G., Bredesen, D.E., Ellerby, H.M., 2002a. Coupling endoplasmic reticulum stress to the cell death program. An Apaf-1-independent intrinsic pathway. J. Biol. Chem. 277, 21836–21842.

Rao, R.V., Peel, A., Logvinova, A., del Rio, G., Hermel, E., Yokota, T., Goldsmith, P.C., Ellerby, L.M., Ellerby, H.M., Bredesen, D.E., 2002b. Coupling endoplasmic reticulum stress to the cell death program: role of the ER chaperone GRP78. FEBS Lett. 514, 122–128.

Reddy, R.K., Maom, C., Baumeister, P., Austin, R.C., Kaufman, R.J., Lee, A.S., 2003. Endoplasmic reticulum chaperone protein GRP78 protects cells from apoptosis induced by topoisomerase inhibitors: role of ATP binding site in suppression of caspase-7 activation. J. Biol. Chem. 278, 20915–20924.

Tagami, S., Eguchi, Y., Kinoshita, M., Takeda, M., Tsujimoto, Y., 2000. A novel protein, RTN-XS, interacts with both Bcl-XL and Bcl-2 on endoplasmic reticulum and reduces their anti-apoptotic activity. Oncogene 19, 5736–5746.

Thornberry, N.A., Lazebnik, Y., 1998. Caspases: enemies within. Science 281, 1312–1316.

Tournier, C., Hess, P., Yang, D.D., Xu, J., Turner, T.K., Nimnual, A., Bar-Sagi, D., Jones, S.N., Flavell, R.A., Davis, R.J., 2000. Requirement of JNK for stress-induced activation of the cytochrome *c*-mediated death pathway. Science 288, 870–874.

Urano, F., Wang, X., Bertolotti, A., Zhang, Y., Chung, P., Harding, H.P., Ron, D., 2000. Coupling of stress in the ER to activation of JNK protein kinases by transmembrane protein kinase IRE1. Science 287, 664–666.

Van de Craen, M., Vandenabeele, P., Declercq, W., Van den Brande, I., Van Loo, G., Molemans, F., Schotte, P., Van Criekinge, W., Beyaert, R., Fiers, W., 1997. Characterization of seven murine caspase family members. FEBS Lett. 403, 61–69.

Wang, K., Yin, X.M., Chao, D.T., Milliman, C.L., Korsmeyer, S.J., 1996. BID: a novel BH3 domain-only death agonist. Genes Dev. 10, 2859–2869.

Yoneda, T., Imaizumi, K., Oono, K., Yui, D., Gomi, F., Katayama, T., Tohyama, M., 2001. Activation of caspase-12, an endoplasmic reticulum (ER) resident caspase, through tumor necrosis factor receptor-associated factor 2-dependent mechanism in response to the ER stress. J. Biol. Chem. 276, 13935–13940.

Zou, H., Henzel, W.J., Liu, X., Lutschg, A., Wang, X., 1997. Apaf-1, a human protein homologous to *C. elegans* CED-4, participates in cytochrome *c*-dependent activation of caspase-3. Cell 90, 405–413.

Zou, H., Li, Y., Liu, X., Wang, X., 1999. An APAF-1.cytochrome *c* multimeric complex is a functional apoptosome that activates procaspase-9. J. Biol. Chem. 274, 11549–11556.

THE JOURNAL OF BIOLOGICAL CHEMISTRY
Vol. 279, No. 51, Issue of December 17, pp. 53427–53434, 2004
Printed in U.S.A.

An RNA-interacting Protein, SYNCRIP (Heterogeneous Nuclear Ribonuclear Protein Q1/NSAP1) Is a Component of mRNA Granule Transported with Inositol 1,4,5-Trisphosphate Receptor Type 1 mRNA in Neuronal Dendrites*[S]

Received for publication, August 24, 2004, and in revised form, October 5, 2004
Published, JBC Papers in Press, October 8, 2004, DOI 10.1074/jbc.M409732200

Hiroko Bannai‡§, Kazumi Fukatsu§, Akihiro Mizutani‡¶, Tohru Natsume‖, Shun-ichiro Iemura‖, Tohru Ikegami§, Takafumi Inoue§¶, and Katsuhiko Mikoshiba‡§¶‡‡**

From the ‡Laboratory for Developmental Neurobiology, Brain Science Institute, RIKEN, 2-1 Hirosawa, Wako, Saitama 351-0198, Japan, §Division of Molecular Neurobiology and ‡‡Division of Neural Signal Information NTT-IMSUT, The Institute of Medical Science, The University of Tokyo, 4-6-1 Shirokanedai, Minato-ku, Tokyo 108-8639 Japan, ¶Calcium Oscillation Project, ICORP, Japan Science and Technology Corp., 3-4-4 Shirokanedai, Minato-ku, Tokyo 108-0071, Japan, and ‖National Institute of Advanced Industrial Science and Technology, Biological Information Research Center, 2-41-6 Ohmi, Kohtoh-ku, Tokyo 135-0064, Japan

mRNA transport and local translation in the neuronal dendrite is implicated in the induction of synaptic plasticity. Recently, we cloned an RNA-interacting protein, SYNCRIP (heterogeneous nuclear ribonuclear protein Q1/NSAP1), that is suggested to be important for the stabilization of mRNA. We report here that SYNCRIP is a component of mRNA granules in rat hippocampal neurons. SYNCRIP was mainly found at cell bodies, but punctate expression patterns in the proximal dendrite were also seen. Time-lapse analysis in living neurons revealed that the granules labeled with fluorescent protein-tagged SYNCRIP were transported bi-directionally within the dendrite at ~0.05 μm/s. Treatment of neurons with nocodazole significantly inhibited the movement of green fluorescent protein-SYNCRIP-positive granules, indicating that the transport of SYNCRIP-containing granules is dependent on microtubules. The distribution of SYNCRIP-containing granules overlapped with that of dendritic RNAs and elongation factor 1α. SYNCRIP was also found to be co-transported with green fluorescent protein-tagged human staufen1 and the 3′-untranslated region of inositol 1,4,5-trisphosphate receptor type 1 mRNA. These results suggest that SYNCRIP is transported within the dendrite as a component of mRNA granules and raise the possibility that mRNA turnover in mRNA granules and the regulation of local protein synthesis in neuronal dendrites may involve SYNCRIP.

Protein synthesis in neurons was long believed to occur only in the cell body, but recent evidence showing the presence of mRNA (for review, see Refs. 1–4) and the capacity for local translation of specific mRNAs in neuronal dendrites (Refs. 5 and 6; for review, see Refs. 7 and 8) has changed this belief. Selective transport and localization of certain types of mRNA and subsequent local protein synthesis in neuronal dendrites are now considered as part of the fundamental mechanisms involved in synaptic plasticity.

Various kinds of mRNA, such as mRNA-coding cytoskeletal proteins (MAP2, β-actin, Arc (activity-regulated cytoskeleton-associated protein), and neurofilament proteins), kinases (*e.g.* the α subunit of Ca^{2+}/CaM[1] kinase II (CaMKIIα)), receptors and channels (glycine receptors, glutamate receptors, and inositol 1,4,5-trisphosphate receptor type 1 (IP_3R1)) have been reported to target dendrites of central nervous system neurons (for review, see Refs.4, 8). Many of the mRNAs listed above are transported to the dendrites as a component of ribonucleoprotein complexes called mRNA granules, which were detected with fluorescent dye SYTO14 (9) and by the *in situ* hybridization technique (10, 11). mRNA granules contain ribosomes and other components of translational machinery (9, 12, 13) as well as various mRNA-binding proteins, including fragile X mental retardation protein (14), staufen (15), testis-brain RNA-binding protein (16), zip code-binding protein 1 (17), and heterogeneous nuclear ribonuclear protein (hnRNP) A2 (18). These mRNA-binding proteins are thought to be responsible for the stability and the translational regulation of mRNAs; however, their actual function in dendrites is poorly understood.

We recently discovered a novel RNA-interacting protein, SYNCRIP (synaptotagmin binding, cytoplasmic RNA-interacting protein (19)) in mouse. A human homolog of SYNCRIP was termed as NSAP1 (20) or hnRNP Q1 (21). SYNCRIP is one of three alternative splicing variants (21) and has high homology to hnRNP R. Interestingly, in contrast to hnRNP R and other splicing variants of SYNCRIP (hnRNP Q2 and Q3), SYNCRIP is distributed throughout the cytosol instead of being localized in the nucleus (19). SYNCRIP binds to RNA *in vitro*, preferen-

* This study was supported by grants from the Ministry of Education, Culture, Sports, Science, and Technology (MEXT) of Japan (to T. Inoue and K. M.), the Ministry of Health, Labor, and Welfare of Japan (to T. Inoue), and the 21st Century Center of Excellence Program, Center for Integrated Brain Medical Science from MEXT of Japan (to K. F.). The costs of publication of this article were defrayed in part by the payment of page charges. This article must therefore be hereby marked "*advertisement*" in accordance with 18 U.S.C. Section 1734 solely to indicate this fact.

[S] The on-line version of this article (available at http://www.jbc.org) contains supplemental Table SI, supplemental Data S1, and the legends for supplemental Movies 1–3.

** To whom correspondence should be addressed: Division of Molecular Neurobiology, The Institute of Medical Science, The University of Tokyo, 4-6-1 Shirokanedai, Minato-Ku, Tokyo, 108-8639, Japan. Tel.: 81-3-5449-5320; Fax: 81-3-5449-5420; E-mail: tinoue@ims.u-tokyo.ac.jp.

[1] The abbreviations used are: CaM, calmodulin; CaMKIIα, α subunit of Ca^{2+}/CaM kinase II; IP_3R1, inositol 1,4,5-trisphosphate receptor type 1; hnRNP, heterogeneous nuclear ribonuclear protein; SYNCRIP, synaptotagmin binding cytoplasmic RNA-interacting protein; PBS, phosphate-buffered saline; GFP, green fluorescent protein; mRFP, monomeric red fluorescent protein; NLS, nuclear localization signal; 3′-UTR, 3′-untranslated region; MS2bs, MS2 phage coat protein binding sequences; EF1α, elongation factor1α; EtBr, ethidium bromide; CCD, charge-coupled device; A2RE, hnRNP A2 response element.

tially to poly (A) or poly (U), in a phosphorylation-dependent manner (19, 22, 23). Although SYNCRIP is reported to be a component of protein complexes that stabilize c-*fos* proto-oncogene mRNA in mammalian culture cells (24), the physiological role of SYNCRIP in the cytoplasm is not yet understood. In this study we performed a proteomic analysis of the protein complexes that associate with SYNCRIP in human kidney cell line 293EBNA and found that SYNCRIP preferentially associated with ribosomal proteins and RNA-binding proteins. We also found that SYNCRIP is a component of mRNA granules containing IP_3R1 mRNA transported within the dendrites in a microtubule-dependent manner.

EXPERIMENTAL PROCEDURES

Proteomic Analysis—Proteomics analysis of the proteins that associate with SYNCRIP was performed as previously described (25–27). In brief, human 293EBNA cells were harvested, washed with phosphate-buffered saline (PBS), and lysed at 24 h after the transfection of cDNA coding FLAG-tagged SYNCRIP. Then the resulting cell lysate was incubated with M2-agarose overnight at 4 °C for immunoprecipitation. The protein-bound agarose beads were washed extensively, and the proteins were eluted with FLAG peptide. The isolated complex was precipitated using mixed methanol and chloroform. After vacuum-drying, the precipitate was digested with *Achromobacter* protease I. The digested peptide mixture were analyzed using a Direct nano flow LC-MSM system as described (26), and protein identification was performed according to the criteria described previously (26).

Construction of Fusion Proteins—FLAG-tagged SYNCRIP was generated by subcloning PCR-amplified DNA fragment coding mouse SYNCRIP (19) fused with FLAG tag to its N terminus into pcDNA3 (Invitrogen). To construct a green fluorescent protein (GFP)-tagged SYNCRIP, the coding sequence of mouse SYNCRIP was subcloned into the PstI/KpnI site of pEGFP-C3 (Clontech, Palo Alto, CA). Monomeric red fluorescent protein (mRFP)-tagged SYNCRIP (mRFP-SYNCRIP) was generated by fusing a mRFP, a gift from Dr. R. Tsien (28), to the N terminus of SYNCRIP with the amino acids Glu-Phe as a linker, which was then subcloned into pcDNA3.1/Zeo I (Invitrogen). To construct GFP-fused human staufen1 (GFP-hStau1), the coding region of hStau1 was amplified from HEP22160 (a gift from Dr. S. Sugano) and subcloned into the XhoI/HindIII site of pEGFP-C1 (Clontech).

NLS-MS2-Venus was generated from pGA14-MS2-GFP (a gift from Dr. R. Singer (29)) and pCS2-Venus (a gift from Dr. A. Miyawaki). A coding sequence of "Venus" (a variant of yellow fluorescent protein (30)) was PCR-amplified with 5′-GTGCGGCCGCTGGTATGAGCAAGGGCGAGG-3′and 5′-CTTGAATTCTTACTTGTACAG-3′ using pCS2-Venus as a template. The NotI-EcoRI digest of the resultant cDNA fragment and the BamHI-NotI digest of pG14-MS2-GFP that corresponded to the coding sequence of MS2 coat protein and nuclear localization signal (NLS) were then introduced into the BamHI/EcoRI site of a mammalian expression vector pCS2+.

To construct the RNA expression vector of the 3′-untranslated regions (3′-UTR) of IP_3R1 (IP_3R1 3′-UTR-MS2bs), we amplified a cDNA fragment of 3′-UTR of mouse IP_3R1 (bases 8579–9041) by PCR using primers 5′-GGCTCGAGGCAAATGAGGCAGAGGGAC-3′, and 5′-GCGGGCCCAACCATTTATTACACGAGTATCAAC-3′. The resulting PCR fragment was subcloned into the XhoI/ApaI site of pcDNA3.1/Zeo+, upstream of which 12 copies of MS2 phage coat protein binding sequences (MS2bs) and the coding sequence of alkaline phosphatase were inserted, and the bovine growth hormone polyadenylation signal downstream to the multicloning site was removed.

Cell Culture and Transfection—Primary cultures of neurons were prepared from hippocampi of 1-day-old Wistar rats by a standard method as described previously (31, 32) and plated on poly-L-lysine (Nacalai Tesque, Kyoto, Japan)-coated coverslips at a density of 4.6×10^4-1.3×10^5 cells/cm^2. Cells were cultured in Neurobasal medium (Invitrogen) supplemented with 2.5 mM L-glutamine (Nacalai Tesque), 2.5% (v/v) B-27 (Invitrogen), and antibiotics (250 units/ml penicillin and 250 μg/ml streptomycin). The cultures were transfected with 10 μg of DNAs by a standard calcium phosphate method (33) or 2.5 μg of DNAs by lipofection using Lipofectamine 2000 (Invitrogen) (34) on days 5–6 *in vitro*. For the labeling of 3′-UTR of IP_3R1 mRNA, 0.6 μg of NLS-MS2-Venus and 1.8 μg of IP_3R1 3′-UTR-MS2bs were co-transfected by lipofection. The transfected cells were used for immunohistochemistry or imaging experiments 2–3 days after the transfection, which corresponded to days 7–9 *in vitro*.

Antibodies—The rabbit antibody recognizing the N-terminal region of SYNCRIP, anti-SYNCRIP-N antibody, was obtained as described previously (19). Anti-SYNCRIP-N was used after affinity purification, and the specificity of this antibody has been confirmed by parallel experiments using preimmune serum or anti-SYNCRIP-N antibody preincubated with an excess amount of antigenic polypeptide (19). Anti-elongation factor1α (EF1α) antibody was from Upstate Biotechnology (Charlottesville, VA, clone CBP-KK1). Alexa 488- or Alexa 594-conjugated secondary antibody was from Molecular Probes (Eugene, OR).

Immunohistochemistry, Cell Labeling Experiments, and Confocal Imaging—For immunohistochemistry of native hippocampus, Wistar rats were deeply anesthetized on postnatal day 7 and perfused with 4% paraformaldehyde in PBS. Whole brains were removed and post-fixed in the same fixative overnight at 4 °C. Sagittal sections (thickness, 100 μm) were cut with a Vibratome-type micro slicer (DTK-1500; Dosaka EM, Kyoto, Japan), collected in PBS, and permeabilized with 0.3% Triton X-100. After incubating with blocking solution (1% bovine serum albumin and 0.3% Triton X-100 in PBS) sections were incubated with anti-SYNCRIP-N antibody (1:1000 dilution) in blocking solution overnight at 4 °C and subsequently with Alexa 488-conjugated anti rabbit IgG (Molecular Probes) for 3 h at room temperature. Finally, sections were mounted on slides with Vectashield (Vector Laboratories, Burlingame, CA) and observed under a confocal-scanning microscope (FV-300; Olympus, Tokyo, Japan) attached to an inverted microscope (IX70; Olympus) with a ×10 objective (NA 0.30; Olympus) and a ×40 objective (NA 0.85; Olympus).

For immunostaining of cultured neurons, cells were fixed with 4% formaldehyde in PBS for 10 min. After permeabilization with 0.1% Triton X-100 in PBS for 10 min and blocking with 5% skim milk in PBS, the cells were incubated with the primary antibodies at 1:1000 dilution for anti-SYNCRIP-N antibody and at 1:400 dilution for anti-EF1α antibody. Alexa 488- or Alexa 594-conjugated IgGs (Molecular Probes) were used as secondary antibodies. RNA labeling with ethidium bromide (EtBr) was performed as described previously (35). RNase treatment was conducted by incubating neurons with 20 μg/ml RNase A (Nippongene, Tokyo, Japan) for 15 min after the EtBr staining. For labeling hippocampal neurons with endosomal and lysosomal markers, cells were incubated with 1 mg/ml Texas Red-dextran (M_r 3000; Molecular Probes) overnight. Fluorescence images of cultured neurons were taken under a confocal-scanning microscope (FV-300) using a 60× objective (NA 1.4; Olympus).

All of the images taken by the confocal microscope were digitally smoothed to reduce the noise level. The smoothing filter was implemented using 3 × 3 spatial convolutions, where the value of each pixel in the selection was replaced with the weighted average of its 3 × 3 neighborhood. Center pixels are 4-fold weighted over surrounding pixels.

Time-lapse Imaging and Data Analysis—The culture medium was supplemented with 20 mM HEPES (pH 7.3) for the time-lapse imaging experiments. The temperature was maintained at ~37 °C by a heating chamber that surrounded the microscope stage. For single color time-lapse imaging, the cells were visualized under an inverted microscope (IX70, Olympus) and a 60× objective (NA 1.45, Olympus) using standard filter sets and a mercury lamp. Sequential images were acquired with a cooled charge-coupled device (CCD) camera (ORCA-ER; Hamamatsu Photonics, Hamamatsu, Japan) with a 58- or 117-ms exposure time every 10 s. For multicolor time-lapse imaging, neurons were visualized under an inverted microscope (IX81; Olympus) equipped with a motorized fluorescence mirror unit exchanger, standard filter sets, and a 60× objective (NA 1.4; Olympus). Images were taken with a cooled CCD camera (ORCA-ER) with a 200-ms exposure time every 10 s.

Data were analyzed using TI Workbench, which is a custom-made software written by T. Inoue. Positions of fluorescent vesicles were plotted against time, and velocity of the granular movements was obtained by linear fitting of the slope. Only structures moving in more than three image frames were taken into account. The velocities were calculated for each period of consecutive movement. Images of time-lapse (Figs. 3*A*, 6*B*, and 7*C*) presented in this study were subjected to digital smoothing with the same algorithm as the confocal images (see above) to reduce the noise level.

Drug Preparation and Drug Treatment—Stock solutions of nocodazole (10 mg/ml, Sigma) and latrunculin A (1 mg/ml, Molecular Probes) were prepared in dimethyl sulfoxide (Me_2SO) and stored at −20 °C. Neurons were incubated with nocodazole (30 μg/ml) and latrunculin A (1 μg/ml) for 1 h at 37 °C in 5% CO_2. To confirm that the cytoskeleton was disrupted, fixed cells were stained with anti-tubulin antibody (Lab Vision, CA) or Alexa 594-phalloidin (Molecular Probes). We found no

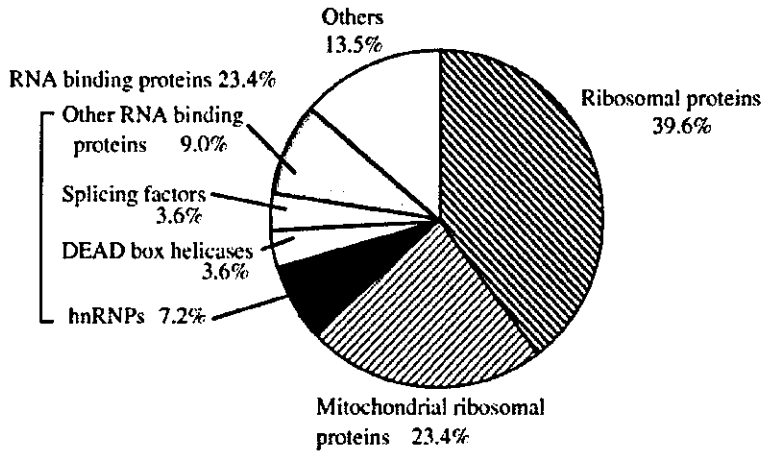

FIG. 1. **Classification of the 111 proteins identified as components of the SYNCRIP-associated protein complexes in 293EBNA cells.** Detailed compositions of each class are shown in supplemental Table SI.

changes in the microtubules or actin structure from control cells exposed to 0.1–0.3% Me_2SO (data not shown).

RESULTS

Proteomic Analysis of SYNCRIP-associated Proteins—Proteins associated with SYNCRIP were isolated by immunoprecipitation from human 293EBNA cells expressing FLAG-tagged SYNCRIP by using anti-FLAG antibody. The 111 proteins listed in supplemental Table SI were identified as components of protein complexes containing FLAG-tagged SYNCRIP. Among these 111 proteins, 44 were identified as ribosomal proteins (39.6%) and 26 were mitochondrial ribosomal proteins (23.4%), which are encoded by nuclear genes and synthesized in the cytosol (36) (Fig. 1 and supplemental Table SI). In addition, 26 RNA-binding proteins (23.4%) including 8 hnRNPs (7.2%), 4 DEAD box helicases (3.6%), and 4 splicing factors (3.6%) were also identified as SYNCRIP-associated proteins. These results suggest that SYNCRIP preferentially associates with protein complexes involved in mRNA processing and translation.

The Distribution and Dynamics of SYNCRIP in Hippocampal Neurons—mRNA granules, the ribonucleoprotein complexes present in neuronal dendrites, have been reported to contain ribosomes and other components of translation machinery (9, 12, 13) as well as a number of RNA-binding proteins (14–18). The above results of proteomic analysis in 293EBNA cells indicate that SYNCRIP preferentially associates with the major component of mRNA granules, that is, ribosomal proteins and RNA-binding proteins (Fig. 1, supplemental Table SI). In addition, SYNCRIP itself has the ability to bind to RNA, preferentially to poly(A) and poly(U) sequences *in vitro* (19, 22, 23). These findings led us to hypothesize that SYNCRIP is a component of the mRNA granules in neuronal dendrites.

To test this hypothesis, we investigated the expression pattern and dynamics of SYNCRIP in the dendrites of rat hippocampal neurons. Expression of SYNCRIP within the hippocampus of rats was investigated by immunohistochemistry using anti-SYCNRIP-N antibodies. SYNCRIP was expressed in the pyramidal cell layer and granular cell layer (Fig. 2*A*), and SYNCRIP signals were mainly observed in the cell bodies of hippocampal neurons (Fig. 2*B*). In addition, the proximal dendrites of pyramidal cells were also labeled with the SYNCRIP antibody (Fig. 2*B*, *arrowheads*). To investigate the localization and dynamics of SYNCRIP in detail, we transfected cultured rat hippocampal neurons with plasmid DNAs encoding mouse SYNCRIP (19) tagged with GFP (GFP-SYNCRIP). To confirm that GFP-SYNCRIP reflects the localization of endogenous SYNCRIP in cultured hippocampal neurons, we compared the immunocytochemical patterns of endogenous SYNCRIP and

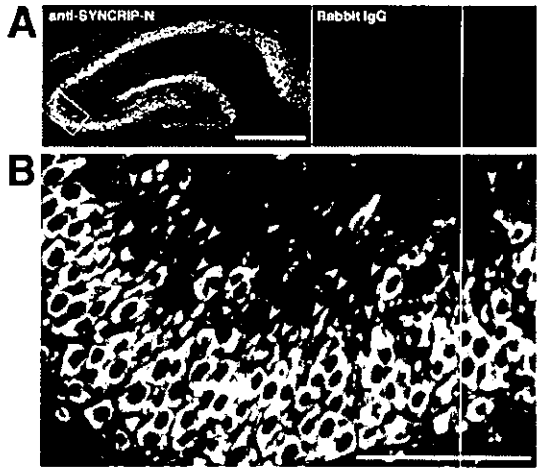

FIG. 2. **Distribution pattern of endogenous SYNCRIP in rat hippocampus.** *A*, *left*, immunohistochemistry with anti-SYNCRIP-N antibody. *Right*, control experiment using nonspecific rabbit IgG. Strong signals for endogenous SYNCRIP were found in the pyramidal and granular layers. *Scale bar*, 500 μm. *B*, a high magnification image of the *boxed* region in *A*. As well as the cell bodies, proximal dendrites of pyramidal neurons were also labeled by anti-SYNCRIP-N antibody (*arrowheads*). Images were taken with a confocal microscope. *Scale bar*, 100 μm.

the distribution of GFP-SYNCRIP signals. Endogenous SYNCRIP was distributed in the dendrites as well as in the cell body of cultured hippocampal neurons (Fig. 3*A*, *left*) as was observed in native tissue. SYNCRIP was found in granules of various sizes in the dendrites (Fig. 3*A*, *right*, *arrowheads*). GFP-SYNCRIP also exhibited a distribution pattern very similar to that of endogenous SYNCRIP (Fig. 3*B*), indicating that the expression pattern of GFP-SYNCRIP reliably reflects that of endogenous SYNCRIP in cultured neurons.

Time-lapse microscopy with a CCD camera revealed that some of the granules labeled with GFP-SYNCRIP traveled within the dendrites (Fig. 4*A* and supplemental Movie 1). Granules labeled with GFP-SYNCRIP moved along the dendrite in both anterograde (to the periphery) and retrograde (to the soma) directions, and a change in direction of movement was observed in some granules (Fig. 4*B*). Double labeling of GFP-SYNCRIP with Texas Red-dextran, which is a marker for endosomes and lysosomes, indicated that the mobile GFP-SYNCRIP-positive granules were not part of the endosome-lysosomal system because GFP-SYNCRIP did not overlap with the Texas Red-dextran signal in either the cell bodies or the dendrites (data not shown). The velocity profile of the GFP-SYN-